



1 A dataset of 10-year regional-scale soil moisture and soil temperature 2 measurements at multiple depths on the Tibetan Plateau

3 Pei Zhang^{1,2}, Donghai Zheng², Rogier van der Velde¹, Jun Wen³, Yaoming Ma², Yijian Zeng¹, Xin
4 Wang⁴, Zuoliang Wang⁴, Jiali Chen^{2,5}, and Zhongbo Su¹

5 ¹Faculty of Geo-Information Science and Earth Observation (ITC), University of Twente, Enschede, 7514AE, the Netherlands

6 ²State Key Laboratory of Tibetan Plateau Earth System, Environment and Resources, Institute of Tibetan Plateau Research,
7 Chinese Academy of Sciences, Beijing, 100101, China

8 ³College of Atmospheric Sciences, Chengdu University of Information Technology, Chengdu, 610225, China

9 ⁴Northwest Institute of Eco-Environment and Resources, Chinese Academy of Sciences, Lanzhou, 730000, China

10 ⁵College of Earth and Environmental Sciences, Lanzhou University, Lanzhou, 730000, China

11

12 *Correspondence:* Donghai Zheng (zhengd@itpcas.ac.cn) and Zhongbo Su (z.su@utwente.nl)

13

14 **Abstract.** Soil moisture and soil temperature (SMST) are important state variables for quantifying exchange of heat and water
15 between land and atmosphere. Yet, long-term regional-scale in-situ SMST measurements are scarce on the Tibetan Plateau
16 (TP), even fewer are available for multiple soil depths. “Tibet-Obs” is such a long-term regional-scale SMST observatory in
17 the TP established 10 years ago that includes three SMST monitoring networks, i.e., Maqu, Naqu, and Ngari (including Ali
18 and Shiquanhe), located in the cold humid area covered by short grasses, the cold semiarid area dominated by tundra, and the
19 cold arid area dominated by desert, respectively. This paper presents a long-term (~10 years) SMST profile dataset collected
20 from the Tibet-Obs, which includes the original in-situ measurements at a 15-min interval collected between 2008 and 2019
21 from all the three networks and the spatially upscaled data (SM_{ups} and ST_{ups}) for the Maqu and Shiquanhe networks. The quality
22 of the upscaled data is proved to be good with errors that are generally better than the measured accuracy of adopted SMST
23 sensors. Long term analysis of the upscaled SMST profile data shows that the amplitudes of SMST variations decrease with
24 increasing soil depth, and the deeper soil layers present later onset of freezing and earlier start of thawing and thus shorter
25 freeze-thaw duration in both Maqu and Shiquanhe networks. In addition, there are notably differences noted between the
26 relationships of SM_{ups} and ST_{ups} under freezing conditions for the Maqu and Shiquanhe networks. No significant trend can be
27 found for the SM_{ups} profile in the warm season (from May to October) for both networks that is consistent with the tendency
28 of precipitation. Similar finding is also found for the ST_{ups} profile and air temperature in the Shiquanhe network during the
29 warm season. For the cold season (from November to April), a drying trend is noted for the SM_{ups} above 20 cm in the Maqu
30 network, while no significant trend is found for those in the Shiquanhe network. Comparisons between the long-term upscaled
31 data and five reanalysis datasets indicate that none of current model-based products can reproduce the seasonal variations and
32 inter-annual trend changes of measured SMST profile dynamics in both networks. All the products underestimate the ST_{ups} at
33 every depth, leading to earlier onset of freezing and later onset of thawing, which essentially demonstrates the current model
34 are not able to adequately simulate winter conditions on the TP. In short, the presented dataset would be valuable for evaluation



35 and improvement of long-term satellite- and model-based SMST products on the TP, enhancing the understanding of TP
36 hydrometeorological processes and their response to climate change. The dataset is available in the 4TU.ResearchData
37 repository at <https://doi.org/10.4121/20141567.v1>.

38 **1 Introduction**

39 Soil moisture and soil temperature (SMST) are important state variables for quantifying water, energy, and carbon exchange
40 processes in the soil-vegetation-atmosphere system (Zheng et al., 2018a; van der Velde et al., 2009). Quantifying the seasonal
41 dynamics and trend changes of the SMST is important to understand the response of hydrological cycle and vegetation
42 dynamics to climate change. Over the past decades, many efforts have been dedicated to obtain worldwide reliable SMST data
43 through in-situ measurements, remote sensing, and model simulations (Dorigo et al., 2011; Entekhabi et al., 2010; Rodell et
44 al., 2004). Thereinto, in-situ measurements are essential for the creation of ground reference for the validation of remote
45 sensing and model-based products (Colliander et al., 2017; Chen et al., 2017; Zeng et al., 2015), as well as improving model
46 parametrizations (Zheng et al., 2017, 2015a, b) and remote sensing retrieval algorithms (Zheng et al., 2019, 2018b). Since the
47 SMST measurements at a single site cannot well represent the value of a satellite pixel or model grid due to spatial variability,
48 several regional-scale monitoring networks were established to collect SMST measurements at regional-scale, some of which
49 are contributing to the International Soil Moisture Network (ISMN) (Dorigo et al., 2011, 2021).

50 Known as the third pole, exchange of water and energy between land and atmosphere on the Tibetan Plateau (TP) plays a
51 crucial role in regulating climate processes in the Northern Hemisphere and the evolution of the Asian monsoon (Wu et al.,
52 1998; Yao et al., 2012). Soil freeze-thaw (F/T) cycle is a typical process on the TP, which has a significant impact on the
53 energy exchange between land and atmosphere as well as water cycle (Zheng et al., 2017, 2018a). Knowledge on SMST
54 seasonal variations, trend changes and the F/T states on the TP can, therefore, contribute to a better understanding of the Asian
55 monsoon circulation and cryosphere changes. However, SMST monitoring networks are scarce on the TP compared to its vast
56 territory, and even fewer exist with a long time series measurements and/or with measurements at multiple soil depths. To our
57 knowledge, there are only two operational SMST observatories that provide long-term measurements at multiple soil depths
58 on the TP, i.e., Tibet-Obs (Tibetan Plateau observatory of plateau scale SMST) (Su et al., 2011; Zhang et al., 2021) and CTP-
59 SMTMN (Soil Moisture and Temperature Monitoring Network on the central TP) (Yang et al., 2013).

60 The Tibet-Obs is the first operational SMST observatory on the TP that started to provide SMST measurements in 2008, which
61 was designed to provide a representative coverage of distinct climate regimes and land surface conditions across the TP (Su et
62 al., 2011). The Tibet-Obs comprises three in-situ monitoring networks, i.e., Maqu, Naqu, and Ngari (including Ali and
63 Shiquanhe) (Fig. 1), which are respectively located in the cold humid area with cold dry winter and rainy summer covered by
64 short grasses, the cold semiarid area dominated by tundra, and the cold arid area dominated by desert. In the Tibet-Obs, SMST
65 sensors were installed at multiple depths, which facilitate the calibration/validation of satellite-based retrieval algorithms and
66 products, as well as the model-based SMST products. Table 1 summarizes the main applications of the Tibet-Obs SMST data



67 with focus on simultaneous usage of SM and ST measurements or usage of SM/ST measurements at multiple depths for the
68 product validations. A summary related to the usage of only surface SM data is included in Zhang et al. (2021). Based on Table
69 1 and the summary made in Zhang et al. (2021), it may be concluded that the Tibet-Obs data were mainly applied to evaluate
70 surface SM products, whereas a few studies simultaneously evaluated SM and ST products, and even less focused on the
71 investigation of profile dynamics using measurements at multiple depths. In addition, most of previous studies focused on a
72 certain short-term period (e.g., several years) while the Tibet-Obs holds SMST data for more than 10 years (Zhang et al., 2021),
73 and most of current satellite- and model-based products also provide long-term (e.g., ≥ 10 years) SMST data. Moreover,
74 previous assessments were mainly concentrated on estimating error metrics between SMST products and measurements, while
75 how well these SMST products can capture the long-term trend and variations of in-situ SMST dynamics is still unknown.
76 Therefore, development of a long-term dataset of SMST measurements at multiple depths based on the Tibet-Obs is essential
77 to comprehensively assess and improve the reliability of current SMST products regarding to seasonal variations and trend
78 changes, enhancing their applications to improve our understanding on changes of hydrological and cryosphere processes on
79 the TP.

80 In this paper, we present a long-term (~ 10 years) SMST profile dataset collected from the Tibet-Obs, which expands the surface
81 SM dataset introduced by Zhang et al. (2021) to include both SM and ST measurements collected at multiple depths. The
82 analysis of seasonal dynamics and trend as well as validation of model-based products are also extended to multiple depths for
83 an approximately 10-year period. In the Tibet-Obs, Decagon (now: METER Group) EC-TM/5TM probes and EM50 data
84 loggers were deployed for each site at multiple depths (e.g., 5, 10, 20, 40, 60 or 80 cm below the surface) to record SMST
85 profile measurements with a 15-minute interval. The presented SMST profile dataset includes in-situ measurements collected
86 between May 2008 and August 2019 for all three networks of the Tibet-Obs, and spatially upscaled data for the Maqu and
87 Shiquanhe networks.

88 The objective of this paper is two folds: 1) to describe the long-term in-situ SMST profile dataset including its generation and
89 validation, and 2) to demonstrate its uniqueness for evaluating model-based SMST profile products for a long-term period
90 (~ 10 years). The paper is organized as follows: Section 2 describes the in-situ SMST measurements collected from the Tibet-
91 Obs, as well as other data used in this research including meteorological data and model-based products. Section 3 presents
92 the spatial upscaling method, data pre-processing steps, statistical performance metrics, and Mann-Kendall trend test methods.
93 The preliminary analysis and applications of the SMST profile dataset are presented in Section 4. The information of data
94 availability is shown in Section 5. Finally, the conclusions are drawn in Section 6.



95 **2 Data**

96 **2.1 Tibet-Obs network and in-situ SMST profile measurements**

97 **2.1.1 Network design and instrumentation**

98 The Tibet-Obs was originally established in 2008 and includes three regional-scale SMST monitoring networks (Fig. 1): the
99 Maqu network at the eastern TP located in cold humid climate area, the Naqu network in the central TP located in cold semiarid
100 climate area, and the Ngari network (including Ali and Shiquanhe) in the western TP located in cold arid climate area. Each
101 network includes various numbers of in-situ SMST monitoring sites, and each monitoring site is configured with one Decagon
102 EM50 data logger and several Decagon SMST probes (i.e., EC-TM and 5TM) to record SMST profile dynamics every 15-
103 minute. The SMST probes were installed with the pins inserted in horizontal direction at multiple depths up to 80 cm (see Fig.
104 1f). The measured range of the ST sensor is from -40 to 60 °C at 0.1 °C resolution with ± 1 °C accuracy. The SM sensor
105 measures liquid water content at a $0.0008 \text{ m}^3 \text{ m}^{-3}$ resolution with $\pm 0.03 \text{ m}^3 \text{ m}^{-3}$ accuracy. The accuracy of the SM sensor was
106 further improved via a soil-specific calibration, leading to a root mean square difference (RMSD) of about $0.02 \text{ m}^3 \text{ m}^{-3}$ (Dente
107 et al., 2012). Nominally instruments maintenance, battery replacement, and data collection took place every year. Several
108 initially established SMST monitoring sites were damaged by local people or animals, and there are more than 15 sites newly
109 installed between 2014 and 2016 (see Figs. A1-A3). Therefore, there are only few monitoring sites that could provide long-
110 term continuous SMST data records throughout the period from 2008 to 2019. Brief descriptions of SMST profile data records
111 at each monitoring network are further provided in the following subsections, and additional information about the Tibet-Obs
112 can be found in Zhang et al. (2021) and Su et al. (2011).

113 **2.1.2 Maqu network**

114 The Maqu network is located in the headwaters of the Yellow River (33.60°-34.20°N, 101.70°-102.70°E) with a land cover
115 dominated by short grasses. It covers a large river valley and its surroundings have elevations varying from 3400 to 3800 m
116 above sea level (a.s.l). Its annual mean air temperature is about 1.2 °C and precipitation is around 600 mm per year. The Maqu
117 network includes 26 SMST monitoring sites and covers an area of approximately 40 km by 80 km (Fig. 1b). There are 13 sites
118 collecting SMST measurements at depths of 5, 10, 20, 40 and 80 cm, 4 sites with measurements at 5, 10, 20, and 40 cm, one
119 site with measurements at 5, 10, and 20 cm, and 8 sites with measurements at 5 and 10 cm. The corresponding data length for
120 every depth of each site is presented in Fig. A1 for every year from May 2008 to May 2019. Eight initially established
121 monitoring sites were damaged before 2015, and 6 new sites were installed between 2014 and 2016. Fig. 2a shows further the
122 number of available monitoring sites for collecting SMST measurements at different depths in the Maqu network for every
123 month between 2008 and 2019. The number of available monitoring sites providing SMST measurements of 5 cm is up to 19
124 in 2009, which however, decreased as time progressed. The number of sites providing SMST measurements of 10 cm is
125 comparable to that of 5 cm, but the SMST measurements at 20, 40, and 80 cm depths are considerably less. It can be found
126 that the period between May 2010 and May 2011 contains the largest number of available monitoring sites. Among all the



127 sites, the CST05 and NST01 sites provide with 11 years of data the longest records of SMST measurements for depths of 5,
128 10, 20, 40, and 80 cm from 2008 to 2019 (see Fig. A1).

129 **2.1.3 Ngari network**

130 The Ngari network is located in the Ngari prefecture and includes the Shiquanhe and Ali networks. The land cover of the
131 network is dominated by desert system at elevations varying from 4200 to 4700 m **a.s.l.** Its annual mean air temperature is
132 about 7.0 °C and precipitation is less than 100 mm per year. The Shiquanhe network situated in vicinity of the Shiquanhe
133 county (32.36°-32.76°N, 79.75°-80.25°E), which includes 20 monitoring sites and covers an area of approximately 30 km by
134 40 km (Fig. 1d). There are 9 sites collecting the SMST measurements at depths of 5, 10, 20, 40, and 60 cm, 9 sites with
135 measurements at 5, 10, 20, and 40 cm, and 2 sites with measurements at 5, 10, and 20 cm. The corresponding data length for
136 every depth of each site is presented in Fig. A2 for every year from August 2010 to August 2019. Six initially established
137 monitoring sites were damaged before 2016, and 5 new sites were installed in 2016. Fig. 2b shows further the number of
138 available monitoring sites for collecting SMST measurements at different depths in the Shiquanhe network every month
139 between 2010 and 2019. The number of available monitoring sites providing SMST measurements of 5 cm is up to 14 in 2010,
140 which then decreased as time progressed until 2016 when new additional sites were installed, making the total up to 13 sites
141 in 2017. The number of sites proving SMST measurements of 10, 20, and 40 cm are comparable to that of 5 cm, which is,
142 however, significantly less for the SMST measurements at 60 cm. It can be also found that the period between August 2017
143 and August 2018 contains the largest number of available monitoring sites. Among all the sites, the SQ03 and SQ14 sites
144 provide with 10 years of data the longest records of SMST measurements for depths of 5, 10, 20, and 40 cm from 2010 to 2019
145 (see Fig. A2). The Ali network is located near the Ngari station for the Desert Environment Observation and Research of the
146 Chinese Academy of Science (NASDE/CAS) (33.30°-33.50°N, 79.60°-79.80°E). It consists of 4 monitoring sites (Fig. 1c) that
147 all collect the SMST measurements at depths of 5, 10, 20, 40, and 60 cm. The corresponding data length for every depth and
148 each site are presented in Fig. A2 for every year from August 2010 to August 2019 as well. Fig. 2c shows further the number
149 of available monitoring sites for collecting SMST measurements at different depths in the Ali network every month between
150 2010 and 2018. It can be found that the number of available monitoring sites providing SMST measurements for every depth
151 is generally less than 4 and the valid data records are not continuous, and thus the Ali network will not be used for further
152 analysis in this study.

153 **2.1.4 Naqu network**

154 The Naqu network is located in the Naqu River basin (31.20°-31.40°N, 91.75°-92.15°E) with a land cover dominated by
155 grassland (tundra). It covers a flat terrain with rolling hills at 4500 m a.s.l. on average. It exhibits the dry winter and rainy
156 summer receiving about 400 mm precipitation per year. The Naqu network includes 11 SMST monitoring sites (Fig. 1e) that
157 all collect the SMST measurements at around 5, 10, 20, 40, and 60 cm depths. The corresponding data length for every depth
158 of each site is presented in Fig. A3 for every year from June 2010 to August 2019. Three initially established monitoring sites



159 were damaged before 2016, and 4 new sites were installed in 2016. Fig. 2d shows further the number of available monitoring
160 sites for collecting SMST measurements at different depths in the Naqu network every month between 2010 and 2019. The
161 number of available monitoring sites providing SMST measurements for every depth is generally less than 4 before 2016,
162 which increased significantly after 2016 but with continuous valid data of less than 2 years. Therefore, the SMST data in the
163 Naqu network will also not be used for further analysis in this study.

164 **2.2 Meteorological data**

165 Precipitation and air temperature used in this study for the Maqu and Shiquanhe networks are obtained from the meteorological
166 dataset provided by the China Meteorological Administration (CMA). The dataset includes air pressure, air temperature,
167 evaporation, precipitation, relative humidity, sunshine duration, and wind speed, which were collected by the automatic
168 weather stations. The daily precipitation and air temperature collected at the Maqu (34.00°N, 102.08°E) and Shiquanhe
169 (32.50°N, 80.08°E) weather stations are used for comparison with the time series of SMST profile data, and the corresponding
170 monthly values are used for trend analysis. The daily precipitation is the cumulative value for the period between 20h of the
171 previous day and 20h of the current day in Beijing time, while the daily air temperature is the mean value. The monthly
172 precipitation is calculated by summing the daily precipitation, while the monthly mean air temperature is the average of daily
173 air temperature within each month.

174 **2.3 Model-based SMST products**

175 Basic information of selected model-based SMST products is given in Table 2, and brief descriptions of each product are
176 provided in the following subsections.

177 **2.3.1 ERA5**

178 The ERA5 is a reanalysis product obtained through the assimilation of as many observations as possible in the upper air and
179 near surface. The SMST data are available from 1979 till present, with a grid spacing of $0.25^{\circ} \times 0.25^{\circ}$ and a temporal resolution
180 of hourly. The SMST data of the top three model layers are used in this study, which represent the soil depths of 0-7, 7-28,
181 and 28-100 cm, respectively. The ERA5 product is available in the Climate Change Service (CSC) Climate Data Store (CDS)
182 at <https://cds.climate.copernicus.eu/cdsapp#!/dataset/reanalysis-era5-single-levels?tab=form> (last access: 27th June 2022).
183 More information about the ERA5 product can be found in Hersbach et al. (2020).

184 **2.3.2 GLDAS-2.1 CLSM**

185 The GLDAS-2.1 CLSM product (Global Land Data Assimilation System Version 2 Catchment Land Surface Model) is based
186 on simulations by the Catchment-F2.5 land surface model (LSM) performed with the Land Information System (LIS) Version
187 7. The SMST data are available from 2000 till present, with a grid resolution of $1.0^{\circ} \times 1.0^{\circ}$ and at a time interval of 3-hour. The
188 ST data for the depths of 0-10, 10-29, and 29-68 cm are selected in this study, and the surface SM (0-2 cm) and rootzone SM



189 (0-100 cm) data are also used. The GLDAS-2.1 CLSM product is available in the Goddard Earth Science Data and Information
190 Services Center (GES DISC) at https://disc.gsfc.nasa.gov/datasets/GLDAS_CLSM10_3H_2.1/summary (last access: 27th June
191 2022). More information about the GLDAS product can be found in Rodell et al. (2004).

192 **2.3.3 GLDAS-2.1 Noah**

193 The GLDAS-2.1 Noah product is based on the Noah LSM version 3.6 simulations performed with the LIS Version 7. The
194 SMST data are available from 2000 to present, with a grid resolution of 0.25°*0.25° and with a 3-hour interval. The SMST
195 data for the depths of 0-10, 10-40, and 40-100 cm are used in this study. The GLDAS-2.1 Noah product is available in the
196 GES DISC at https://disc.gsfc.nasa.gov/datasets/GLDAS_NOAH025_3H_2.1/summary (last access: 27th June 2022).

197 **2.3.4 GLDAS-2.1 VIC**

198 The GLDAS-2.1 VIC (Variable Infiltration Capacity) product is based on the VIC 4.1.2 LSM simulations performed with the
199 LIS Version 7. The coverage period, grid spacing and time interval of the SMST data are the same as the GLDAS-2.1 CLSM
200 product. The SMST data of the first and second model layers are selected in this study. The surface layer has a 30 cm depth,
201 whereas the depth of second layer varies with region that is about 30-130 cm for our study areas as can be found at
202 <https://ldas.gsfc.nasa.gov/gldas/specifications> (last access: 27th June 2022). The GLDAS-2.1 VIC product is available in the
203 GES DISC at https://disc.gsfc.nasa.gov/datasets/GLDAS_VIC10_3H_2.1/summary (last access: 27th June 2022).

204 **2.3.5 MERRA2**

205 The MERRA2 (Modern-Era Retrospective analysis for Research and Applications version 2) is the latest version of global
206 atmospheric reanalysis product, which uses the Goddard Earth Observing System Model (GEOS) version 5.12.4. The SMST
207 data are available from 1980 to present, with a grid size of 0.5°*0.625° and hourly interval. The ST data of the top three model
208 layers as well as SM data of surface (0-5 cm) and rootzone (0-100 cm) are selected in this study. The layer thicknesses of
209 model layers for the ST data also varies with region, which are 0-10, 10-30, and 30-70 cm for our study areas as can be found
210 at https://disc.gsfc.nasa.gov/datasets/M2C0NXLND_5.12.4/summary (last access: 27th Feb 2022). The MERRA2 product is
211 available in the GES DISC at https://disc.gsfc.nasa.gov/datasets/M2T1NXLND_5.12.4/summary (last access: 27th June 2022).
212 More information about the MERRA2 product can be found in Gelaro et al. (2017).

213 **3 Methods**

214 **3.1 Production and uncertainty analysis of upscaled SMST profile dataset**

215 Spatial upscaling is used to create regional-scale SMST data from in-situ measurements collected at individual location that
216 matched with the spatial domain of satellite-based and model-based products. Zhang et al. (2021) demonstrated the good



217 performance of the **arithmetic averaging approach** in upscaling the surface SM of the Tibet-Obs network, which is also adopted
218 in this study to obtain the regional-scale SMST profile data for Maqu and Shiquanhe.

219 The arithmetic averaging method assigns equal weights to each SMST monitoring site of the network, which can be formulated
220 as:

$$221 X_t^{ups} = \frac{1}{M} \sum_{i=1}^M X_{t,i}^{obs} \quad (1)$$

222 where t represents the time in days, i represents the i^{th} SMST monitoring site, M represents the total number of monitoring
223 sites, X_t^{ups} stands for the upscaled SMST, and $X_{t,i}^{obs}$ is the SMST measurements for the i^{th} site.

224 Considering that the number of available SMST monitoring sites in the Tibet-Obs network generally changes with time (see
225 Fig. 2), Zhang et al. (2021) suggested to use only the sites that provide the longest continuous measurements to obtain the
226 long-term upscaled dataset. They also showed that the upscaled surface SM with input of all active monitoring sites regardless
227 of the continuity tends to produce an inconsistent trend. Therefore, we use the sites of Maqu and Shiquanhe networks that have
228 the longest records of SMST profile data from 2009 to 2019 to produce the long-term upscaled dataset. Specifically,
229 measurements collected from the CST05 and NST01 sites in the Maqu network are selected to produce the long-term regional-
230 scale SMST dataset for depths of 5, 20, 40, and 80 cm for the period between May 2009 and May 2019. The measurements at
231 the 10 cm are not used for the upscaling because the sensor at the 10 cm of CST05 site was changed one time in the mid of
232 May 2011 which leads to a discontinuity in the collected time series. As in **Zhang et al. (2021)**, the measurements collected in
233 the year with the largest number of available monitoring sites, i.e., May 2010 and May 2011 for the Maqu network (see Fig.
234 2), are used to preliminarily quantify the uncertainty of upscaled SMST profile data, whereby the average of the measurements
235 at all the available sites are treated as ground reference for the Maqu network. Similarly, measurements collected from the
236 SQ03 and SQ14 sites in the Shiquanhe network are selected to produce the long-term regional-scale SMST dataset for depths
237 of 5, 10, 20, and 40 cm for the period between August 2010 and August 2019 since both sites only provide SMST profile
238 measurements up to 40 cm. The average of measurements collected at the period between August 2017 and August 2018 that
239 has the largest number of available sites are used to quantify the uncertainty of upscaled SMST data in the Shiquanhe network.

240 3.2 Pre-processing of model-based products

241 We select five widely-used model-based products (see Section 2.3) which contain both SM and ST profile simulations. To
242 make an objective evaluation of these products using the Tibet-Obs in-situ SMST data, some essential pre-processing steps
243 are undertaken regarding to three aspects: unify time interval and units of SMST simulations, determine number of model
244 grids that cover the in-situ network, and match the model layers to the depths of in-situ measurements.

245 The units of SM data from the GLDAS-2.1 CLSM, Noah, and VIC products is **converted from “kg m⁻²” to “m³ m⁻³”**, and the
246 units for the ERA5 and MERRA2 SM data is already with “m³ m⁻³”. The units of ST data from all the model-based products
247 is converted from “K” to “C”. The hourly or 3-hour SMST data from all the products are averaged to daily values. We define
248 the period between 1st May and 31st October as the warm season, and the period between 1st November of the previous year



249 and 30th April of the following year as the cold season. The ERA5, GLDAS-2.1 CLSM and VIC SM data in the cold seasons
250 are excluded for the analysis in this study since their values represent the total soil water content including both liquid water
251 and ice content, while the in-situ SM data only provide measurements of liquid water content.
252 All the model grids falling into the scope of in-situ network are extracted from each product. Afterwards, the native grids of
253 each product are downscaled to 0.25°*0.25° sub-grid cells using a bilinear interpolation. Subsequently, the SMST data in all
254 the sub-grid cells falling into the scope of in-situ network are averaged to match the upscaled in-situ SMST data that represent
255 the regional-scale mean values of in-situ network (see Fig. B1).
256 To match the depths of in-situ SMST measurements, the model-based SMST data are resampled across the vertical soil profile
257 using the linear interpolation method. We assume that the SMST values of each model layer are representative for the mid-
258 point of this layer. For example, the SMST for the layer of 10-40 cm in the GLDAS-2.1 Noah product are representative for
259 the depth of 25 cm. The detailed calculation processes are presented in the Appendix B.

260 3.3 Statistical indicator

261 Four statistical indicators are used in this study for the evaluation of upscaled in-situ SMST data as well as the model-based
262 products, including Bias, root-mean-square-difference (RMSD), unbiased RMSD, and Pearson correlation coefficient (R).
263 They can be formulated as:

$$264 \text{ Bias} = \frac{\sum_{t=1}^n (X_t^{est} - X_t^{obs})}{N} \quad (2)$$

$$265 \text{ RMSD} = \sqrt{\frac{\sum_{t=1}^n (X_t^{obs} - X_t^{est})^2}{N}} \quad (3)$$

$$266 \text{ ubRMSD} = \sqrt{\text{RMSD}^2 - \text{Bias}^2} \quad (4)$$

$$267 R = \frac{\sum_{t=1}^n (X_t^{obs} - \overline{X^{obs}})(X_t^{est} - \overline{X^{est}})}{\sqrt{\sum_{t=1}^n (X_t^{obs} - \overline{X^{obs}})^2} \sqrt{\sum_{t=1}^n (X_t^{est} - \overline{X^{est}})^2}} \quad (5)$$

268 where N denotes the number of data points. For the evaluation of upscaled in-situ SMST data, X_t^{obs} represents the mean SMST
269 of the largest number of available monitoring sites in a certain year for each in-situ network (see Section 3.1), and X_t^{est}
270 represents the upscaled SMST based on the monitoring sites that provide the longest continuous measurements as input. For
271 the assessment of model-based products, X_t^{obs} represents the upscaled SMST for each in-situ network, and X_t^{est} represents the
272 SMST simulations derived from each product.

273 3.4 Trend analysis

274 The Mann Kendall trend test is used in this study to determine whether a trend is presented within the long-term SMST time
275 series derived either from the upscaled in-situ measurements or from the model-based products. The trend analysis is also
276 performed for the precipitation and air temperature data for comparison purposes. The trend analysis is respectively carried
277 out over the warm season, the cold season, and the full year. Therefore, the data points are monthly mean values of each year



278 for calculating seasonal statistics instead of annual mean value, and all missing data points are assigned an equal value smaller
279 than existed valid data points. If the trend test results show a significant upward or downward tendency, the Sen's slope
280 estimate method is adopted to quantify the magnitude of the tendency. A detailed description of the trend analysis process can
281 be found in Appendix C.

282 **4 Results**

283 Section 4.1 presents the upscaled SMST profile data for the Maqu and Shiquanhe networks spanning the 10-year period from
284 2010 to 2019 (see Section 3.1), as well as the analysis results for the SMST seasonal dynamics, trend test, detection of F/T
285 state and soil freezing characteristics at different depths. The uncertainty analysis results for the upscaled SMST profile data
286 are given in Section 4.2. Application of the upscaled data to evaluate the performance of model-based products is presented in
287 Section 4.3 to demonstrate its suitability for the evaluation of readily available SMST profile products.

288 **4.1 Analysis of the upscaled SMST profile measurements**

289 **4.1.1 Maqu network**

290 Figs. 3a and 3c show the time series of upscaled daily SM (SM_{ups}) and ST (ST_{ups}) at depths of 5, 20, 40, and 80 cm from
291 January 2010 to December 2018 for the Maqu network, respectively. The daily precipitation (P) and air temperature (T_a)
292 collected from the Maqu weather station (Fig. 1b) are also shown for comparison purposes. The time series of the SM_{ups} at
293 different depths shows similar seasonal variations, with high values in warm summer with larger amounts of rainfall and low
294 values in cold winter with soil freezing and much smaller amounts of snowfall. The amplitudes of SM_{ups} variations generally
295 decrease with increasing soil depth, with larger variations noted for soil layers above 20 cm, and smallest one at the deepest
296 depth of 80 cm. The soil layers below 20 cm are dryer than the upper layers in the warm season. The time series of the ST_{ups}
297 at different depths also show similar seasonality with peak values in summer and lowest values in winter that is in agreement
298 with the seasonal T_a dynamics. The soil layers above 40 cm generally drop below 0 °C in winter, while the ST_{ups} of 80 cm is
299 always greater than 0 °C throughout the year, indicating that the maximum freezing depth in the Maqu network is shallower
300 than 80 cm. The magnitude of ST_{ups} variations also diminish with increasing soil depth.

301 Figs. 3b and 3d further show the SM_{ups} and ST_{ups} profile dynamics with 15-min interval for a single year between May 2010
302 and May 2011, which confirm that amplitudes of both SM_{ups} and ST_{ups} variations decrease with depth. The SM_{ups} variations at
303 5 and 20 cm are comparable to each other and larger than those at 40 and 80 cm, which also show better response to the
304 precipitation in rainy season. Obvious diurnal cycles can be noted for the ST_{ups} at 5 cm, which diminish with depth and are
305 virtually absent at 40 cm. The ST_{ups} at 5 cm starts to drop below 0 °C around mid-November, leading to a sharp decrease of
306 surface SM_{ups} due to freezing of the soil. The deeper layers gradually freeze as time progresses, and the freezing depths reach
307 its peak around mid-February. Later on, the soil starts thawing with a sharp increase of SM_{ups} as the ST_{ups} rises above 0 °C,
308 and the entire soil profile is totally thawed around the mid-April. In general, both start date of soil freezing and end date of soil



309 thawing increase with increasing soil depth. To further explore the characteristics of F/T cycle in the Maqu network, Fig. 3e
310 shows the freezing start day (FSD), thawing end day (TED), and F/T duration of each year for the depths of 5, 20 and 40 cm
311 during the study period, and the 80 cm layer does not freeze (see Figs. 3c and 3d). The FSD is defined as the first day that the
312 daily ST drops below 0 °C along with sharp SM decrease in current year, and the TED is the last day of ST below 0 °C in next
313 year. The number of days between the FSD and TED is referred to as the F/T duration. There is no specific information of the
314 FSD and TED in 2017 for the depths of 5 and 20 cm due to missing data of in-situ ST measurements in this period, and the
315 same holds for the soil depth of 40 cm between 2015 and 2018 (see Figs 2a and A1). It can be observed that the inter-annual
316 variabilities of the FSD, TED, and F/T duration for each depth are within 30 days, and no significant trend is found. It also
317 confirms that the deeper layer generally shows late onset of freezing and an earlier start of thawing every year leading to
318 shorter F/T duration.

319 Figs. 4a and 4b show the Mann Kendall trend test and Sen's slope estimate for the 9-year (2010-2018) SM_{ups} and ST_{ups} at
320 depths of 5 and 20 cm for the Maqu network in the warm season, cold season, and full year. The trend analysis for the depth
321 of 40 cm is not presented since there is not long enough (< 7 years) continuous SMST time series due to missing data. The
322 trends of the P and T_a are also shown in Figs. 4a and 4b, respectively. As described in Section 3.4, the time series would present
323 a significant trend if the absolute value of statistic Z is greater than 1.96 in this study. The results show that no significant trend
324 is found for the SM_{ups} at 5 and 20 cm in the warm season like the P . For the cold season, the SM_{ups} at depths of 5 and 20 cm
325 show a drying trend despite the absence of a P trend. Consequently, the SM_{ups} at 5 and 20 cm in the full year also show a
326 drying trend with the Sen's slopes of -0.004 and -0.002, respectively, which is in agreement with the P trend. The ST_{ups} at
327 depth of 5 cm shows a decreasing trend in the warm season while no significant trend is found for the T_a and ST_{ups} at 20 cm.
328 In the cold season, there is no significant trend found for the T_a and ST_{ups} at 5 and 20 cm. For the full year, the ST_{ups} at 5 cm
329 shows a decreasing trend with a Sen's slope of -0.08 while no significant trend found for the ST_{ups} at 20 cm like the T_a .

330 Fig. 5 shows the soil freezing characteristics for the depths of 5, 20 and 40 cm for the Maqu network by plotting the ST_{ups}
331 against corresponding measured unfrozen SM for all subzero temperatures during the freezing and thawing periods in the cold
332 season. The power function fitting curves to the soil freezing characteristics and corresponding fitting parameters are given in
333 figure for both freezing and thawing periods. The difference between the soil freezing characteristics of freezing and thawing
334 periods is much smaller at the surface layer (i.e., 5 cm), which increases with increasing soil depth. At the deeper soil layers
335 (e.g., 20 and 40 cm), the freezing rate (i.e., the amount change of unfrozen SM with temperature) of unfrozen SM with
336 decreasing ST in the freezing period is larger than the thawing rate of ice content with increasing ST during the thawing period.
337 As such, the obtained parameter values of the power function fitting curves are identical to each other at the surface layer for
338 the freezing and thawing periods, which are different for the deeper soil layers. The obtained parameter values are also distinct
339 from each other at different soil layers, indicating the layering characteristics of frozen soil in the Maqu network.



340 4.1.2 Shiquanhe network

341 Figs. 6a and 6c show the time series of daily SM_{ups} and ST_{ups} at depths of 5, 10, 20, and 40 cm from January 2011 to December
342 2018 for the Shiquanhe network, respectively. The daily P and T_a collected from the Shiquanhe weather station (Fig. 1d) are
343 also shown for comparison purposes. The SM_{ups} time series at different depths display the similar seasonality to that found for
344 the Maqu network. The amplitudes of SM_{ups} variations generally decrease with increasing soil depth, with slightly larger
345 variations noted for soil layers above 10 cm, and smallest one at the deepest depth of 40 cm. The layers above 10 cm are dryer
346 than the deeper layers in the warm season expect for the rainy period. The time series of the ST_{ups} at different depths also show
347 the similar seasonality to that found for the Maqu network, whereas the amplitudes of ST_{ups} variations are larger than those of
348 the Maqu network and diminish with soil depth. The soil layers above 40 cm generally drop below 0 °C in winter, indicating
349 that the maximum freezing depth in the Shiquanhe network is deeper than 40 cm.

350 Figs. 6b and 6d further show the SM_{ups} and ST_{ups} profile dynamics with 15-min interval for a single year between August 2017
351 and August 2018, which confirm that amplitudes of both SM_{ups} and ST_{ups} variations decrease with depth. The SM_{ups} variations
352 at 5 and 10 cm are comparable to each other and larger than those at 20 and 40 cm, which also show better response to the
353 precipitation. Obvious diurnal cycles can be noted for the ST_{ups} at 5, 10, and 20 cm, which diminish with depth and are almost
354 absent at 40 cm. The ST_{ups} at 5 and 10 cm starts to drop below 0 °C around early November, leading to a decrease of SM_{ups}
355 due to soil freezing. The deeper layers freeze as time progresses, and the freeze depths reach its maximum around early January.
356 Later on, the soil starts thawing with an increase of SM_{ups} when the ST_{ups} rises above 0 °C, and the entire soil profile is totally
357 thawed around mid-March. To further explore the characteristics of F/T cycles in Shiquanhe, Fig. 6e shows the FSD, TED,
358 and F/T duration of each year for the depths of 5, 10, 20, and 40 cm during the study period. There is no specific information
359 of the FSD and TED in 2011 and 2013 for the depth of 5 cm due to missing data of in-situ ST measurements in this period,
360 and the same holds for the soil depths of 20 and 40 cm in 2018 (see Figs 2b and A2). In general, the FSD increases with
361 increasing soil depth whereas the TED is comparable at each depth. It can be observed that the inter-annual variabilities of the
362 FSD, TED, and F/T duration for each depth are within 20 days, and there is no significant trend found for them. It also confirms
363 that the F/T cycles at 5 and 10 cm are almost the same with each other, and the deeper layers (i.e., 20 and 40 cm) generally
364 show late onset of freezing, leading to shorter duration.

365 Figs. 7a and 7b show the trend analysis results for the 8-year (2011-2018) SM_{ups} and ST_{ups} at depths of 5, 20, and 40 cm for the
366 Shiquanhe network in the warm season, cold season, and full year. The trends of the P and T_a are also shown in Fig. 7a and
367 7b, respectively. The results show that no significant trend is found for the SM_{ups} at all three depths in the warm season, which
368 is in agreement with the P trend. Meanwhile, the SM_{ups} at 5 and 20 cm also do not show a significant trend in the cold season
369 like the P , whereas the SM_{ups} at 40 cm shows a wetting trend. Consequently, the SM_{ups} at 40 cm shows a wetting trend with a
370 Sen's slope of 0.001 while no trend found for the P and SM_{ups} at 5 and 20 cm for the full year. The ST_{ups} at all three depths do
371 not show a significant trend in the warm season, while an increasing trend is found in the cold season, which is in agreement



372 with T_a trend. For the full year, no trend is found for the ST_{ups} at depths of 5 and 20 cm like T_a , while an increasing trend is
373 found for ST_{ups} of 40 cm.

374 Fig. 8 shows the soil freezing characteristics for the depths of 5, 20 and 40 cm for the Shiquanhe network. The fitted power
375 functions to the soil freezing characteristics and the corresponding parameters are also given for the freezing and thawing
376 periods. It is observed that there is no notable difference between the soil freezing characteristic of freezing and thawing
377 periods at each depth. As such, the obtained parameter values of the power function fitting curves are identical for the freezing
378 and thawing periods. However, the obtained parameter values are distinct from each other at different soil layers, indicating
379 the layering characteristics of frozen soil in the Shiquanhe network.

380 **4.2 Uncertainty analysis of the upscaled SMST profile dataset**

381 The spatial upscaling data is inevitably subject to uncertainty as a result of the SMST spatial variabilities. Therefore, in this
382 section we quantify the uncertainties of the long-term upscaled SMST profile dataset for the Maqu and Shiquanhe networks
383 via comparisons to the mean of SM and ST measurements collected during the year with the largest number of active
384 monitoring sites that is considered as the “ground truth” (hereafter SM_{tru} and ST_{tru}) as shown in Zhang et al. (2021) (see Section
385 3.1). The selected validation periods are from 16 May 2010 to 15 May 2011 and from 1 September 2017 to 31 August 2018
386 for the Maqu and Shiquanhe networks, respectively.

387 Fig. 9a shows the comparisons between the time series of SM_{ups} and SM_{tru} at soil depths of 5, 20, and 40 cm with 15-min
388 interval for the Maqu network from 16 May 2010 to 15 May 2011, and the comparisons between the ST_{ups} and ST_{tru} profile
389 dynamics are shown in Fig. 9b. The statistical performance metrics, i.e., bias, RMSD, ubRMSD, and R, computed between
390 the upscaled SMST and the ground truth are shown in the figure as well. In general, the variations of SM_{ups} and SM_{tru} are
391 consistent with each other at every depth as indicated by very high R values (≥ 0.985), yielding RMSD values of 0.025, 0.019,
392 and $0.030 \text{ m}^3 \text{ m}^{-3}$ at the depths of 5, 20, and 40 cm, respectively. These RMSD values are comparable and even better than the
393 measurement accuracy (see Section 2.1), indicating the good performance for the SM_{ups} profile data. The consistency between
394 the ST_{ups} and ST_{tru} variations is even better as indicated by higher R values (≥ 0.995) for each soil depth, yielding RMSD values
395 of 0.7, 0.2, and $0.3 \text{ }^\circ\text{C}$ at the depths of 5, 20, and 40 cm, respectively. These RMSD values are also better than the reported
396 accuracy of temperature measurements (see Section 2.1), implying the good performance for the ST_{ups} profile data as well.
397 Table 3 presents further the FSD, TED, and F/T duration for 5, 20, and 40 cm soil depths estimated based on the upscaled
398 SMST profile data and ground truth, respectively. The estimated FSD, TED, and F/T duration are close to each other especially
399 at upper soil layers (e.g., 5 and 20 cm), and the noted differences for the FSD and TED are generally less than 3 days except
400 that of TED at 40 cm, leading to differences of not more than 4 days for the F/T duration.

401 Fig. 10a shows the comparisons between the time series of SM_{ups} and SM_{tru} at soil depths of 5, 20, and 40 cm with 15-min
402 interval for the Shiquanhe network from 1 September 2017 to the 31 August 2018, and the comparisons between the ST_{ups} and
403 ST_{tru} profile dynamics are shown in Fig. 10b. The statistical performance metrics are shown in the figures as well. Similar to
404 the Maqu network, the variations of SM_{ups} and SM_{tru} are consistent with each other for each soil depth as indicated by high R



405 values (> 0.92), yielding RMSD values of 0.011, 0.009, and 0.010 $\text{m}^3 \text{m}^{-3}$ at the depths of 5, 20, and 40 cm, respectively. These
406 RMSD values are much better than the measured accuracy of adopted SM sensor (see Section 2.1), indicating the good
407 performance for the SM_{ups} profile data. The consistence between the ST_{ups} and ST_{tru} variations is even better as indicated by
408 higher R value (≥ 0.97) for every soil depth. Table 3 presents further the FSD, TED, and F/T duration for 5, 20, and 40 cm soil
409 depths estimated based on the upscaled SMST profile data and ground truth, respectively. The estimated FSD, TED, and F/T
410 duration are close to each other especially at upper soil layers (e.g., 5 and 20 cm), and there is little difference for the FSD and
411 TED except that of TED at 40 cm, leading to differences of not more than 8 days for the F/T duration.

412 4.3 Application of the upscaled SMST profile dataset to validate model-based products

413 **To demonstrate the uniqueness of the upscaled SMST profile dataset for validating existing products for a long-term period,**
414 the performance of five model-based products is investigated in this section, including the ERA5, MERRA2, GLDAS-2.1
415 CLSM (hereafter CLSM), GLDAS-2.1 Noah (hereafter Noah), and GLDAS-2.1 VIC (hereafter VIC) (see Section 2.3). The
416 performance of these model-based products in capturing the SMST seasonal variations, long-term trend changes, and the F/T
417 cycle at depths of 5, 20, and 40 cm in the Maqu and Shiquanhe networks is evaluated. The cold season SM data of the ERA5,
418 CLSM, and VIC products are excluded for the analysis since their values represent the total soil water content while the in-
419 situ sensors can measure the liquid soil water content in frozen soil.

420 4.3.1 Maqu network

421 Figs. 11a-11c show the time series of daily average SM at soil depths of 5, 20, and 40 cm derived from the SM_{ups} and the five
422 model-based products from January 2010 to December 2018 for the Maqu network. The error metrics, i.e., bias, RMSD,
423 ubRMSD, and R, computed between the five model-based SM data and the SM_{ups} for the warm and cold season are listed in
424 Table 4. Among the five model-based products, the ERA5 SM product agrees best with the SM_{ups} at 5 and 20 cm in the warm
425 season with the lowest RMSD values of 0.053 and 0.032 $\text{m}^3 \text{m}^{-3}$ and the largest R values of 0.76 and 0.74, but it tends to
426 overestimate the SM_{ups} at 40 cm with a bias of 0.108 $\text{m}^3 \text{m}^{-3}$. Similarly, the VIC SM product is also able to capture the magnitude
427 of SM_{ups} dynamics at 5 and 20 cm in the warm season with slightly larger RMSD values of 0.060 and 0.049 $\text{m}^3 \text{m}^{-3}$, but also
428 overestimates the SM_{ups} at 40 cm with a bias of 0.088 $\text{m}^3 \text{m}^{-3}$. The other three products tend to considerably underestimate the
429 SM_{ups} at 5 and 20 cm in the warm season, but they yield better estimates of the SM at 40 cm as indicated by smaller biases and
430 RMSD values. In the cold season, the Noah SM product generally captures well the SM_{ups} variations at surface layer (i.e., 5
431 cm) but overestimates the SM_{ups} at deeper layers (e.g., 20 and 40 cm), and overestimations are also found for the MERRA2
432 products at all the depth. The trend analysis results for the five model-based SM data are also presented in Fig. 4a. The results
433 show that no significant trend is found for any of five model-based SM products at every depth in the warm season, which is
434 in agreement with the trend of SM_{ups} . Both Noah and MERRA2 SM products are able to reproduce the drying trend noted for
435 the SM_{ups} in the cold season and full year except for the Noah SM product of 5 cm.



436 Figs. 11d-11f show the time series of monthly average ST at soil depths of 5, 20, and 40 cm derived from the ST_{ups} and the
437 five model-based products for the Maqu network. The corresponding error metrics computed by daily ST_{ups} are listed in Table
438 4 as well. In general, the five model-based ST products have similar performance and can well capture the seasonal variations
439 of ST_{ups} at every depth. However, they tend to underestimate the ST_{ups} across the entire study period, and the magnitude of
440 underestimations generally increases with increasing soil depths. The trend analysis results for the five model-based ST data
441 are also presented in Fig. 4b. At the surface layer (i.e., 5 cm), only the VIC ST product shows a decreasing trend in the warm
442 season like the ST_{ups} , while no significant trend is found for other products. In the cold season, there is no significant trend
443 presented for the CLSM, Noah, and MERRA2 ST products at surface layer that is consistent with ST_{ups} , while the other two
444 products show a decreasing trend. For the full year, the Noah and VIC ST products are able to reproduce the decreasing trend
445 found for the ST_{ups} of 5 cm, whereas no significant trend is found for other products. The trends for the deeper soil layers (i.e.,
446 20 and 40 cm depths) are consistent with each other for each model-based ST product, and there is no significant trend found
447 for the products in both warm and cold season like that ST_{ups} , expect the VIC ST product shows a decreasing trend.
448 Consequently, the ERA5, CLSM, and MERRA2 ST products do not show significant trend at deeper layers in the full year,
449 that is consistent with ST_{ups} , whereas the VIC product of two depths and Noah product of 20 cm show a decreasing trend for
450 the full year.

451 To further investigate the performance of five model-based products in capturing the characteristics of F/T cycle in the Maqu
452 network, Fig. 12 shows the FSD, TED, and F/T duration derived from the five model-based products and upscaled dataset for
453 each year during the study period. It can be observed that all the five model-based products underestimate the FSD especially
454 at deeper depths. The FSD estimated based on the upscaled dataset generally increases with increasing depth, while those
455 estimates using the model-based products are close to each other at different depth. In contrast to the FSD, all the products
456 overestimate the TED at deeper depths. In other words, all the model-based products tend to produce earlier onset of freezing
457 and later onset of thawing, leading to longer F/T duration in comparison to the upscaled dataset. The soil freezing
458 characteristics for depths of 5, 20 and 40 cm obtained based on the Noah and MERRA2 products are shown in Fig. 5 as well.
459 It can be observed that the difference between the soil freezing characteristics of freezing and thawing periods generally
460 decreases with increasing soil depth for the two models that is inconsistent with the upscaled dataset. In comparison to the
461 upscaled dataset, both Noah and MERRA2 products tend to produce higher unfrozen SM values at the same subzero ST in the
462 freezing period, and overestimations are also found in the thawing period except that of Noah model at 5 cm. This can explain
463 why the two models overestimate the SM_{ups} in the cold season especially at deeper depths as shown in Fig. 11.

464 4.3.2 Shiquanhe network

465 Figs. 13a-13c show the time series of daily average SM at soil depths of 5, 20, and 40 cm derived from the SM_{ups} and the five
466 model-based products from January 2011 to December 2018 for the Shiquanhe network. The error metrics computed between
467 the five model-based SM data and the SM_{ups} for the warm and cold season are listed in Table 5. Among the five model-based
468 SM products, the ERA5 product agrees best with the SM_{ups} at 5 cm in the warm season with the lowest RMSD of $0.06 \text{ m}^3 \text{ m}^{-3}$



469 and largest R value of 0.80, while other products tend to overestimate the SM_{ups} especially for the VIC product. Both the Noah
470 and MERRA2 products also overestimate the SM_{ups} of 5 cm in the cold season. For the 20 and 40 cm deeper depths, all the
471 products systematically overestimate the SM_{ups} , among which the ERA5 product shows the lowest bias while the VIC product
472 presents the largest bias. The trend analysis results for the five model-based SM data are also presented in Fig. 7a. The results
473 show that no significant trend is found for the MERRA2 product at every depth throughout the year, that is consistent with the
474 SM_{ups} of upper layers (i.e., 5 and 20 cm), whereas both CLSM and VIC products show a drying trend at each depth. At soil
475 depths of 5 cm, there is also no significant trend found for the ERA5 and Noah products like the SM_{ups} , while the ERA5
476 product shows a drying trend at deeper layers (i.e. 20 and 40 cm) in the warm season, and Noah product also presents a drying
477 trend at deeper layers for the cold season and full year, both of which are inconsistent with those of SM_{ups} .

478 Figs. 13d-13f show the time series of monthly average ST at soil depths of 5, 20, and 40 cm derived from the ST_{ups} and the five
479 model-based ST products from January 2011 to December 2018 for the Shiquanhe network. The corresponding error metrics
480 computed by daily ST_{ups} are also listed in Table 5. Similar to the Maqu network, all the five model-based products well capture
481 the seasonal variations of ST_{ups} at every depth, but they tend to underestimate the ST_{ups} throughout the entire study period, and
482 the magnitude of underestimations also increases with increasing soil depth. Among all the products, the Noah and CLSM
483 products yields the lowest bias and RMSD in the warm and cold seasons, respectively, while the VIC product presents the
484 largest bias for both seasons. It should be noted that the Noah product is slight worse than the CLSM product in the cold
485 season. The trend analysis results for the five model-based ST data are also presented in Fig. 7b. The results show that all
486 products do not show significant trend at every depth in the warm season that is consistent with the ST_{ups} . In the cold season,
487 the ERA5, CLSM, and MERRA2 products show an increasing trend at every depth that is consistent with the ST_{ups} , while no
488 significant trend is found for the VIC product. An increasing trend is also noted for the Noah product of 5 and 20 cm despite
489 no trend is found at 40 cm. For the full year, only the ERA5 and MERRA2 products capture the trends of ST_{ups} at all three
490 depths. At the depth of 5 and 20 cm, except the CLSM product, no significant trend is found for other products that is consistent
491 with the ST_{ups} . For the depth of 40 cm, besides the Noah and VIC products, an increasing trend is found for other products and
492 the ST_{ups} .

493 To further investigate the performance of five model-based products in capturing the characteristics of F/T cycle in the
494 Shiquanhe network, Fig. 14 shows the FSD, TED, and F/T duration derived from the five model-based products and upscaled
495 dataset for each year during the study period. Similar as the Maqu network, all the model-based products tend to produce
496 earlier onset of freezing and later onset of thawing at every depth, leading to underestimation of FSD and overestimation of
497 TED and thus longer F/T duration in comparison to the upscaled dataset. Among the five model-based products, the CLSM
498 product provides the closet estimates of TED and F/T duration compared to the upscaled dataset, while the VIC product
499 presents the worst performance. The soil freezing characteristics for the depths of 5, 20, and 40 cm obtained from the Noah
500 and MERRA2 products are shown in Fig. 8 as well. Similar to the Maqu network, both Noah and MERRA2 products tend to
501 produce higher unfrozen SM values at the same subzero ST in both freezing and thawing periods, leading to the overestimation



502 of SM in the cold season in comparison to the upscaled dataset (see Fig. 13), and the magnitude of overestimation increases
503 with increasing soil depth.

504 **5 Data availability**

505 A long-term (2008-2019) dataset of SMST at multiple depths on the TP is freely available from the 4TU.ResearchData
506 repository at <https://doi.org/10.4121/20141567.v1> (Zhang et al., 2022). The original in-situ SMST data, the upscaled SMST
507 data, and the supplementary data are stored in .xlsx files. A user guide document is given to introduce the content of the dataset
508 and to provide the method to download online datasets used in this paper.

509 **6 Conclusions**

510 The Tibet-Obs is a long-term SMST observatory in the TP covering different representative climatic and land surface
511 conditions, which includes the Maqu, Naqu, and Ngari (including Ali and Shiquanhe) networks. The three networks are located
512 in the cold humid area covered by short grass, the polar area dominated by tundra, and the cold arid area dominated by desert,
513 respectively. Each network includes various numbers of in situ SMST monitoring sites, and each monitoring site is configured
514 with one Decagon (now: METER group) EM50 data logger and several Decagon SMST probes (i.e., EC-TM and 5TM) to
515 monitor SMST dynamics at multiple depths (e.g., 5, 10, 20, 40, and 60/80 cm underground) every 15-minute, which have
516 generally been in operation for over a decade. This paper presents a long-term (~10 years) SMST profile dataset collected from
517 the Tibet-Obs, which includes original in-situ measurements collected between 2008 and 2019 from all the three networks and
518 the spatially upscaled data (SM_{ups} and ST_{ups}) for the Maqu and Shiquanhe networks. The uncertainty of the spatially upscaled
519 dataset are further quantified via comparison to the average of SMST measurements collected at a certain year having the
520 largest number of available valid monitoring sites, i.e., ground truth (SM_{tru} and ST_{tru}). The results show that the SM_{ups} and
521 SM_{tru} are consistent with each other at every depth for both Maqu and Shiquanhe networks, yielding RMSD values that are
522 better than the measured accuracy of adopted SM sensor. The variations of ST_{ups} also agree well with the ST_{tru} , and the obtained
523 RMSD value is also better than the measured accuracy of adopted ST sensor in the Maqu network. Therefore, it can be
524 concluded that the quality of the upscaled dataset is generally good.

525 Based on the upscaled dataset, the analysis on the seasonal variations and inter-annual trend changes of profile SMST
526 dynamics, as well as the characteristics of F/T cycle in an approximately 10-year period is carried out for the two
527 hydrometeorologically contrasting networks. The results show that the time series of both SM_{ups} and ST_{ups} at each depth display
528 notable seasonality with peak values in warm summer and lowest values in cold winter, and the amplitudes of their variations
529 generally decrease with increasing soil depth for both networks. It can be noted that the amplitudes of the seasonal SM_{ups}
530 variations in the cold-humid Maqu network area are larger than those of the cold-arid Shiquanhe network, whereas the ST_{ups}
531 seasonality is generally stronger within the Shiquanhe measurements. The Mann Kendall trend analysis results demonstrate



532 that no significant trend is found for the SM_{ups} profile in the warm season (from May to October) for both networks that is
533 consistent with the precipitation (P) trend. A similar finding is also found for the ST_{ups} profile and air temperature T_a for the
534 Shiquanhe network during the warm season. For the cold season (from November to April) and the full year, a drying trend is
535 noted for the SM_{ups} above 20 cm in the Maqu network, while no significant trend is found for those in the Shiquanhe network.
536 In general, the deeper soil layers in both networks present later onset of freezing and earlier thawing and thus shorter F/T
537 duration in comparison to the surface layer. The obtained parameter values of the power function fitting curves to the soil
538 freezing characteristics are distinct from each other at different soil layers in both networks, confirming the layering
539 characteristics of frozen soil on the TP.

540 To demonstrate the uniqueness of the upscaled SMST profile dataset for validating existing products for a long-term period,
541 the performance of five model-based products is investigated. The results show that none of the model-based products can
542 reproduce the seasonal variations and inter-annual trend changes of profile SMST dynamics, and the characteristics of F/T
543 cycle obtained based on the upscaled dataset. Among the five products, only the ERA5 product captures well the seasonal
544 variations and trend changes of SM_{ups} dynamics at surface layer (i.e., 5 cm) during the warm season in both networks, which
545 also provides the lowest bias for the estimations of SM above 20 cm during the warm season. All the products underestimate
546 the ST_{ups} at every depth in both networks, whereby the Noah and ERA5 products provide better estimations in the warm season,
547 and the CLSM and Noah products yield better simulations for the cold season. Consequently, all the model-based products
548 tend to produce earlier onset of freezing and later start of thawing at every depth, leading to underestimation of FSD and
549 overestimation of TED and thus longer F/T duration than observed on the ground.

550 Overall, the Tibet-Obs SMST observatory has greatly advanced the evaluation and improvement of satellite- and model-based
551 SM and ST products for their applications to the TP over the past decade (see Table 1). Development of the long-term (~10
552 years) SMST profile dataset collected from the Tibet-Obs is urgently needed to further strengthen relevant research and could
553 be of value for calibration and validation of long-term satellite- or/and model-based SMST products, improving the
554 representation of TP hydrometeorological processes in current land surface model and satellite-based SM retrieval algorithms,
555 and other applications across scientific disciplines such hydrology, meteorology and climatology.

556 **Author contribution**

557 Pei Zhang, Donghai Zheng, Rogier van der Velde and Zhongbo Su designed the framework of this work. Pei Zhang performed
558 the computations and data analysis, and wrote the manuscript. Donghai Zheng, Rogier van der Velde, and Zhongbo Su
559 supervised the progress of this work and provided critical suggestions, and revised the manuscript. Zhongbo Su, Jun Wen, and
560 Yaoming Ma designed the setup of Tibet-Obs, Yijian Zeng, XinWang and Zuoliang Wang involved in maintaining the Tibet-
561 Obs and downloading the original measurements. Pei Zhang, Zuoliang Wang, and Jiali Chen organized the data.



562 Competing interests

563 The authors declare that they have no conflict of interest.

564 Acknowledgments

565 This study was supported by the National Key Research and Development Program of China (grant no. 2021YFB3900104),
566 the Strategic Priority Research Program of the Chinese Academy of Sciences (grant no. XDA20100103) and the National
567 Natural Science Foundation of China (grant nos. 41971308 and 41871273).

568 Reference

- 569 Bhatti, H. A., Rientjes, T., Verhoef, W., and Yaseen, M.: Assessing temporal stability for coarse scale satellite moisture
570 validation in the Maqu area, Tibet, *Sensors* (Basel), 13, 10725–10748, <https://doi.org/10.3390/s130810725>, 2013.
- 571 Bi, H., Ma, J., Zheng, W., and Zeng, J.: Comparison of soil moisture in GLDAS model simulations and in situ observations
572 over the Tibetan Plateau, 121, 2658–2678, <https://doi.org/10.1002/2015JD024131>, 2016.
- 573 Cao, B., Gruber, S., and Zheng, D.: The ERA5-Land soil temperature bias in permafrost regions, 14, 2581–2595,
574 <https://doi.org/10.5194/tc-14-2581-2020>, 2020.
- 575 Chen, Y., Yang, K., Qin, J., Cui, Q., Lu, H., La, Z., Han, M., and Tang, W.: Evaluation of SMAP, SMOS, and AMSR2 soil
576 moisture retrievals against observations from two networks on the Tibetan Plateau, 122, 5780–5792,
577 <https://doi.org/10.1002/2016JD026388>, 2017.
- 578 Colliander, A., Jackson, T. J., Bindlish, R., Chan, S., Das, N., Kim, S. B., Cosh, M. H., Dunbar, R. S., Dang, L., Pashaian, L.,
579 Asanuma, J., Aida, K., Berg, A., Rowlandson, T., Bosch, D., Caldwell, T., Caylor, K., Goodrich, D., al Jassar, H.,
580 Lopez-Baeza, E., Martínez-Fernández, J., González-Zamora, A., Livingston, S., McNairn, H., Pacheco, A.,
581 Moghaddam, M., Montzka, C., Notarnicola, C., Niedrist, G., Pellarin, T., Prueger, J., Pulliainen, J., Rautiainen, K.,
582 Ramos, J., Seyfried, M., Starks, P., Su, Z., Zeng, Y., van der Velde, R., Thibeault, M., Dorigo, W., Vreugdenhil, M.,
583 Walker, J. P., Wu, X., Monerris, A., O’Neill, P. E., Entekhabi, D., Njoku, E. G., and Yueh, S.: Validation of SMAP
584 surface soil moisture products with core validation sites, 191, 215–231, <https://doi.org/10.1016/j.rse.2017.01.021>,
585 2017.
- 586 Deng, M., Meng, X., Lyv, Y., Zhao, L., Li, Z., Hu, Z., and Jing, H.: Comparison of Soil Water and Heat Transfer Modeling
587 Over the Tibetan Plateau Using Two Community Land Surface Model (CLM) Versions, 12, e2020MS002189,
588 <https://doi.org/10.1029/2020MS002189>, 2020.
- 589 Deng, M., Meng, X., Lu, Y., Li, Z., Zhao, L., Hu, Z., Chen, H., Shang, L., Wang, S., and Li, Q.: Impact and Sensitivity Analysis
590 of Soil Water and Heat Transfer Parameterizations in Community Land Surface Model on the Tibetan Plateau, 13,
591 e2021MS002670, <https://doi.org/10.1029/2021MS002670>, 2021.
- 592 Dorigo, W., van Oevelen, P., Wagner, W., Drusch, M., Mecklenburg, S., Robock, A., and Jackson, T.: A New International
593 Network for in Situ Soil Moisture Data, 92, 141–142, <https://doi.org/10.1029/2011EO170001>, 2011.
- 594 Dorigo, W., Himmelbauer, I., Aberer, D., Schremmer, L., Petrakovic, I., Zappa, L., Preimesberger, W., Xaver, A., Annor, F.,
595 Ardö, J., Baldocchi, D., Bitelli, M., Blöschl, G., Bogena, H., Brocca, L., Calvet, J.-C., Camarero, J. J., Capello, G.,
596 Choi, M., Cosh, M. C., van de Giesen, N., Hajdu, I., Ikonen, J., Jensen, K. H., Kanniah, K. D., de Kat, I., Kirchengast,
597 G., Kumar Rai, P., Kyrouac, J., Larson, K., Liu, S., Loew, A., Moghaddam, M., Martínez Fernández, J., Mattar Bader,
598 C., Morbidelli, R., Musial, J. P., Osenga, E., Palecki, M. A., Pellarin, T., Petropoulos, G. P., Pfeil, I., Powers, J.,
599 Robock, A., Rüdiger, C., Rummel, U., Strobel, M., Su, Z., Sullivan, R., Tagesson, T., Varlagin, A., Vreugdenhil, M.,
600 Walker, J., Wen, J., Wenger, F., Wigneron, J. P., Woods, M., Yang, K., Zeng, Y., Zhang, X., Zreda, M., Dietrich, S.,
601 Gruber, A., van Oevelen, P., Wagner, W., Scipal, K., Drusch, M., and Sabia, R.: The International Soil Moisture



- 602 Network: serving Earth system science for over a decade, 25, 5749–5804, <https://doi.org/10.5194/hess-25-5749-2021>,
603 2021.
- 604 Entekhabi, D., Njoku, E. G., O'Neill, P. E., Kellogg, K. H., Crow, W. T., Edelstein, W. N., Entin, J. K., Goodman, S. D.,
605 Jackson, T. J., Johnson, J., Kimball, J., Piepmeier, J. R., Koster, R. D., Martin, N., McDonald, K. C., Moghaddam,
606 M., Moran, S., Reichle, R., Shi, J. C., Spencer, M. W., Thurman, S. W., Tsang, L., and Zyl, J. van: The Soil Moisture
607 Active Passive (SMAP) Mission, 98, 704–716, <https://doi.org/10.1109/JPROC.2010.2043918>, 2010.
- 608 Gelaro, R., McCarty, W., Suárez, M. J., Todling, R., Molod, A., Takacs, L., Randles, C. A., Darmenov, A., Bosilovich, M. G.,
609 Reichle, R., Wargan, K., Coy, L., Cullather, R., Draper, C., Akella, S., Buchard, V., Conaty, A., da Silva, A. M., Gu,
610 W., Kim, G.-K., Koster, R., Lucchesi, R., Merkova, D., Nielsen, J. E., Partyka, G., Pawson, S., Putman, W.,
611 Rienecker, M., Schubert, S. D., Sienkiewicz, M., and Zhao, B.: The Modern-Era Retrospective Analysis for Research
612 and Applications, Version 2 (MERRA-2), 30, 5419–5454, <https://doi.org/10.1175/JCLI-D-16-0758.1>, 2017.
- 613 Hersbach, H., Bell, B., Berrisford, P., Hirahara, S., Horányi, A., Muñoz-Sabater, J., Nicolas, J., Peubey, C., Radu, R., Schepers,
614 D., Simmons, A., Soci, C., Abdalla, S., Abellan, X., Balsamo, G., Bechtold, P., Biavati, G., Bidlot, J., Bonavita, M.,
615 de Chiara, G., Dahlgren, P., Dee, D., Diamantakis, M., Dragani, R., Flemming, J., Forbes, R., Fuentes, M., Geer, A.,
616 Haimberger, L., Healy, S., Hogan, R. J., Hólm, E., Janisková, M., Keeley, S., Laloyaux, P., Lopez, P., Lupu, C.,
617 Radnoti, G., de Rosnay, P., Rozum, I., Vamborg, F., Villaume, S., and Thépaut, J.-N.: The ERA5 global reanalysis,
618 146, 1999–2049, <https://doi.org/10.1002/qj.3803>, 2020.
- 619 Ju, F., An, R., Yang, Z., Huang, L., and Sun, Y.: Assimilating SMOS Brightness Temperature for Hydrologic Model
620 Parameters and Soil Moisture Estimation with an Immune Evolutionary Strategy, 12, <https://doi.org/10.3390/rs1210>
621 -1556, 2020.
- 622 Li, C., Lu, H., Leung, L. R., Yang, K., Li, H., Wang, W., Han, M., and Chen, Y.: Improving Land Surface Temperature
623 Simulation in CoLM Over the Tibetan Plateau Through Fractional Vegetation Cover Derived From a Remotely
624 Sensed Clumping Index and Model-Simulated Leaf Area Index, 124, 2620–2642, <https://doi.org/10.1029/2018JD028>
625 -640, 2019.
- 626 Liu, Y., Jing, W., Sun, S., and Wang, C.: Multi-Scale and Multi-Depth Validation of Soil Moisture From the China Land Data
627 Assimilation System, 14, 9913–9930, <https://doi.org/10.1109/JSTARS.2021.3116583>, 2021.
- 628 Rodell, M., Houser, P. R., Jambor, U., Gottschalck, J., Mitchell, K., Meng, C.-J., Arsenault, K., Cosgrove, B., Radakovich, J.,
629 Bosilovich, M., Entin, J. K., Walker, J. P., Lohmann, D., and Toll, D.: The Global Land Data Assimilation System,
630 *Bull Am Meteorol Soc*, 85, 381–394, <https://doi.org/10.1175/BAMS-85-3-381>, 2004.
- 631 Su, Z., Wen, J., Dente, L., van der Velde, R., Wang, L., Ma, Y., Yang, K., and Hu, Z.: The tibetan plateau observatory of
632 plateau scale soil moisture and soil temperature (Tibet-Obs) for quantifying uncertainties in coarse resolution satellite
633 and model products, 15, 2303–2316, <https://doi.org/10.5194/hess-15-2303-2011>, 2011.
- 634 Su, Z., de Rosnay, P., Wen, J., Wang, L., and Zeng, Y.: Evaluation of ECMWF's soil moisture analyses using observations on
635 the Tibetan Plateau, 118, 5304–5318, <https://doi.org/10.1002/jgrd.50468>, 2013.
- 636 Velde, R., Su, B., Ek, M., Rodell, M., and Ma, Y.: Influence of thermodynamic soil and vegetation parameterizations on the
637 simulation of soil temperature states and surface fluxes by the Noah LSM over a Tibetan plateau site, 13,
638 <https://doi.org/10.5194/hessd-6-455-2009>, 2009.
- 639 Wang, L., Li, X., Chen, Y., Yang, K., Chen, D., Zhou, J., Qi, J., and Huang, J.: Validation of the global land data assimilation
640 system based on measurements of soil temperature profiles, 218–219, 288–297, <https://doi.org/10.1016/j.agrformet>.
641 -2016.01.003, 2016.
- 642 Yang, K., Qin, J., Zhao, L., Chen, Y., Tang, W., Han, M., Lazhu, Chen, Z., Lv, N., Ding, B., Wu, H., and Lin, C.: A Multiscale
643 Soil Moisture and Freeze–Thaw Monitoring Network on the Third Pole, *Bull Am Meteorol Soc*, 94, 1907–1916,
644 <https://doi.org/10.1175/BAMS-D-12-00203.1>, 2013.
- 645 Yao, T., Thompson, L. G., Mosbrugger, V., Zhang, F., Ma, Y., Luo, T., Xu, B., Yang, X., Joswiak, D. R., Wang, W., Joswiak,
646 M. E., Devkota, L. P., Tayal, S., Jilani, R., and Fayziev, R.: Third Pole Environment (TPE), 3, 52–64,
647 <https://doi.org/10.1016/j.envdev.2012.04.002>, 2012.
- 648 Zeng, J., Li, Z., Chen, Q., Bi, H., Qiu, J., and Zou, P.: Evaluation of remotely sensed and reanalysis soil moisture products
649 over the Tibetan Plateau using in-situ observations, 163, 91–110, <https://doi.org/10.1016/j.rse.2015.03.008>, 2015.



- 650 Zhang, P., Zheng, D., van der Velde, R., Wen, J., Ma, Y., Zeng, Y., Wang, X., Wang, Z., Chen, J., and Su, Z.: A dataset of 10-
651 year regional-scale soil moisture and soil temperature measurements at multiple depths on the Tibetan Plateau.
652 4TU.ResearchData. Dataset. <https://doi.org/10.4121/20141567.v1>, 2022.
- 653 Zhang, P., Zheng, D., van der Velde, R., Wen, J., Zeng, Y., Wang, X., Wang, Z., Chen, J., and Su, Z.: Status of the Tibetan
654 Plateau observatory (Tibet-Obs) and a 10-year (2009–2019) surface soil moisture dataset, 13, 3075–3102,
655 <https://doi.org/10.5194/essd-13-3075-2021>, 2021.
- 656 Zheng, D., van der Velde, R., Su, Z., Wang, X., Wen, J., Booiij, M. J., Hoekstra, A. Y., and Chen, Y.: Augmentations to the
657 Noah Model Physics for Application to the Yellow River Source Area. Part II: Turbulent Heat Fluxes and Soil Heat
658 Transport, 16, 2677–2694, <https://doi.org/10.1175/JHM-D-14-0199.1>, 2015a.
- 659 Zheng, D., van der Velde, R., Su, Z., Wang, X., Wen, J., Booiij, M. J., Hoekstra, A. Y., and Chen, Y.: Augmentations to the
660 Noah Model Physics for Application to the Yellow River Source Area. Part I: Soil Water Flow, 16, 2659–2676,
661 <https://doi.org/10.1175/JHM-D-14-0198.1>, 2015b.
- 662 Zheng, D., der Velde, R., Su, Z., Wen, J., Wang, X., Booiij, M. J., Hoekstra, A. Y., Lv, S., Zhang, Y., and Ek, M. B.: Impacts
663 of Noah model physics on catchment-scale runoff simulations, 121, 807–832, <https://doi.org/10.1002/2015JD023695>,
664 2016.
- 665 Zheng, D., van der Velde, R., Su, Z., Wen, J., Wang, X., and Yang, K.: Evaluation of Noah Frozen Soil Parameterization for
666 Application to a Tibetan Meadow Ecosystem, 18, 1749–1763, <https://doi.org/10.1175/JHM-D-16-0199.1>, 2017.
- 667 Zheng, D., van der Velde, R., Su, Z., Wen, J., Wang, X., and Yang, K.: Impact of soil freeze-thaw mechanism on the runoff
668 dynamics of two Tibetan rivers, 563, 382–394, <https://doi.org/10.1016/j.jhydrol.2018.06.024>, 2018a.
- 669 Zheng, D., Wang, X., van der Velde, R., Ferrazzoli, P., Wen, J., Wang, Z., Schwank, M., Colliander, A., Bindlish, R., and Su,
670 Z.: Impact of surface roughness, vegetation opacity and soil permittivity on L-band microwave emission and soil
671 moisture retrieval in the third pole environment, 209, 633–647, <https://doi.org/10.1016/j.rse.2018.03.011>, 2018b.
- 672 Zheng, D., Li, X., Wang, X., Wang, Z., Wen, J., van der Velde, R., Schwank, M., and Su, Z.: Sampling depth of L-band
673 radiometer measurements of soil moisture and freeze-thaw dynamics on the Tibetan Plateau, 226, 16–25,
674 <https://doi.org/10.1016/j.rse.2019.03.029>, 2019.
- 675 Zhuang, R., Zeng, Y., Manfreda, S., and Su, Z.: Quantifying Long-Term Land Surface and Root Zone Soil Moisture over
676 Tibetan Plateau, 12, <https://doi.org/10.3390/rs12030509>, 2020.
- 677
678
679
680
681
682
683
684
685
686
687
688
689
690
691
692



693 **Table 1. Summary of the applications of Tibet-Obs SMST data and corresponding findings.**

Literature	In-situ data	Satellite- and/or model-based products/simulations	Key findings
Simultaneous usage of SM and ST			
Zheng et al. (2016)	SMST at 5, 10, 20, 40, and 80 cm depths from the Maqu network, period between 2009 and 2010.	SMST simulations by the Noah model including three sets of augmentations.	The augmentations for the turbulent and soil heat transport improved the ST profile simulations, while the augmentations for the soil water flow mitigated deficiencies of SM profile simulations by Noah model.
Deng et al. (2020)	SMST at 5, 10, 20, and 40 cm depths from the Maqu network, period between 2010 and 2011.	SMST simulations by two versions of the Community Land Model (CLM), i.e., versions 4.5 and 5.0.	The ST simulations from both CLM model versions coincided with the in-situ measurements, while the SM simulations showed large biases.
Deng et al. (2021)	SMST at 5 cm depth from the Maqu network during period of 2011 and from the Ngari network during period between 2013 and 2014.	SMST simulations by the CLM5.0 that include nine experiments evaluating soil water and heat transfer parameterizations.	(i) At the Ngari network, ST simulations in all experiments generally coincided with the observations yielding RMSE within 3°C, while SM simulations in Experiment 6 (i.e., replaced soil property data, adopted virtual temperature scheme and dry surface scheme) showed the best performance. (ii) At the Maqu network, ST simulations in Experiment 5 (i.e., replaced soil property data, adopted Balland and Arp scheme and dry surface scheme) showed the best performance, while SM simulations in Experiment 1 (i.e., replaced soil property data) showed the best performance.
Usage of SM at multiple depths			
Su et al. (2013)	SM at 5, 10, 20, 40, and 80 cm depths from the Maqu network, period between 2008 and 2009; SM around 5, 10, 20, 40, and 60 cm depths from the Naqu network, period of 2008.	SM simulations by the European Centre for Medium-Range Weather Forecasts (ECMWF) based on optimum interpolation scheme and point-wise extended Kalman filter scheme, respectively.	(i) At the Naqu network, both ECMWF's SM products showed significant overestimations in the monsoon season, indicating the ECMWF model and soil texture parameter need to be improved for the cold-semiarid area on the TP. (ii) At the Maqu network, both ECMWF's SM products generally showed good and comparable performance in the humid monsoon period.
Bhatti et al. (2013)	SM at 5, 10, 20, 40, and 80 cm depths from the Maqu network, period of 2009.	Advanced Microwave Scanning Radiometer-Earth Observing System (AMSR-E) SM product generated by the Vrije University Amsterdam and NASA.	The in-situ SM measurements at 10 cm are more suitable to validate the AMSR-E SM product.
Bi et al. (2016)	SM at 5, 10, 20, 40, and 80 cm depths from the Maqu network, period between 2008 and 2010.	SM products generated by CLM, Noah, Mosaic, and VIC models implemented in Global Land Data Assimilation System V1 (GLDAS-1) and Noah model adopted in GLDAS-2.	(i) The GLDAS-2 SM product did not show better performance than the GLDAS-1 products. (ii) All four models can capture well the temporal variations of in-situ SM measurements but underestimated the SM values, and the Mosaic model yielded the largest bias.



Ju et al. (2020)	SM at 5 and 40 cm depths from the Maqu network, period between 2011 and 2012.	SM simulations by Variable Infiltration Capacity (VIC) model with assimilation of brightness temperature (T_B) data from the Soil Moisture and Ocean Salinity (SMOS) mission.	Assimilation of SMOS T_B data improved the performance of VIC SM product indicated by reducing the root mean square difference (RMSD) for the SM at 5 cm from 0.126 to 0.087 $m^3 m^{-3}$, which however, had a slight positive impact for the SM at 40 cm.
Zhuang et al. (2020)	SM at 5, 10, 20, 40, and 60/80 cm depths from the Maqu, Naqu, and Ngari networks, period between 2013 and 2016.	Surface SM (SSM) data generated by using the blend method, and then rootzone SM (RZSM) data generated by Cumulative Distribution Function (CDF) matching approach and Soil Moisture Analytical Relationship (SMAR) model based on the blended SSM data.	(i) The blended SSM product constrained by in-situ SM measurements can eliminate the influence of different LSM simulations. (ii) Both SMAR model and CDF matching approach can give reliable RZSM estimates, but the performances varied from different regions, e.g., the SMAR model provided better estimates in the semi-arid area while the CDF matching approach performed slightly better in the arid area.
Liu et al. (2021)	SM at 5, 10, 20, and 40 cm depths from the Maqu and Ngari networks, period between 2013 and 2015.	China Meteorological Administrational Land Data Assimilation System (CLDAS) and GLDAS SM products	The CLDAS and GLDAS SM data can capture the temporal dynamics with favorable performances, expect for the GLDAS SM data at the layer of 10-40 cm
Usage of ST			
Wang et al. (2016)	ST at 5 cm depth from the Maqu network, period between 2008 and 2009.	ST simulations by Noah and CLM models from GLDAS-1, and by Noah model from GLDAS-2	GLDAS-1 CLM product overestimated the ST, while both GLDAS-1 and GLDAS-2 Noah products showed underestimations although they can replicate the daily variability of in-situ ST measurements.
Li et al. (2019)	ST at 5 m depth from the Maqu and Ngari networks, period between 2010 and 2011.	ST simulations by Common Land Model (CoLM) implementing three different fractional vegetation cover (FVC) schemes.	(i) At the Ngari network dominated by sparse grassland or desert, ST simulations were not sensitive to FVC scheme. (ii) At the Maqu network dominated by grass, ST simulations were improved by implementing a new FVC scheme.
Cao et al. (2020)	ST at 5, 10, 20, and 40 cm depths from the Maqu network, period between 2008 and 2016	ERA5-land ST product.	ERA5-land ST data showed a negative bias in the TP, and it matched better to in-situ ST measurements in permafrost regions than in non-permafrost regions.

694
 695
 696
 697
 698
 699
 700
 701
 702
 703



704 **Table 2. Information for the selected model-based products.**

Product	Spatial Resolution	Temporal Resolution	Temporal Coverage	SM Stratification (cm)	ST Stratification (cm)
ERA5	0.25°×0.25°	Hourly	1979 ongoing	0-7, 7-28, 28-100, 100-289	
Noah				0-10, 10-40, 40-100	
CLSM	1°×1°	3 Hours	2000 ongoing	0-2, 0-100	0-10, 10-29, 29-68, 68-144
VIC					0-30, 30-130*, 130-150*
MERRA2	0.5°×0.625°	Hourly	1980 ongoing	0-5*, 0-100*	0-10*, 10-30*, 30-70*, 70-146*

705 * The depth of this layer varies with region, and the value shown here is for our study area.

706 **Table 3. Estimation of FSD, TED, and F/T duration at soil depths of 5, 20, and 40 cm using the upscaled SMST profile dataset and**
 707 **ground truth in the selected single year for the Maqu and Shiquanhe networks.**

	SMST _{ups}			SMST _{tru}		
	5 cm	20 cm	40 cm	5 cm	20 cm	40 cm
Maqu network						
FSD	19 Nov	10 Dec	23 Dec	16 Nov	8 Dec	26 Dec
TED	24 Mar	5 Mar	3 Mar	23 Mar	7 Mar	10 Mar
F/T duration	125	85	70	127	89	74
Shiquanhe network						
FSD	14 Nov	17 Nov	23 Nov	14 Nov	18 Nov	23 Nov
TED	18 Mar	18 Mar	13 Mar	18 Mar	18 Mar	21 Mar
F/T duration	124	121	110	124	120	118

708

709 **Table 4. Statistical indicators of model-based SMST products at soil depths of 5, 20, and 40 cm for the Maqu network in the warm**
 710 **and cold season, respectively.**

		Warm season				Cold season			
		Bias	RMSD	ubRMSD	R	Bias	RMSD	ubRMSD	R
Soil moisture									
5cm	ERA5	0.036	0.053	0.039	0.76	-	-	-	-
	GLDAS CLSM	-0.081	0.098	0.056	0.35	-	-	-	-
	GLDAS Noah	-0.102	0.116	0.055	0.42	-0.047	0.088	0.075	0.52
	GLDAS VIC	0.000	0.060	0.060	0.38	-	-	-	-
	MERRA2	-0.092	0.104	0.049	0.58	0.009	0.089	0.088	0.05
20cm	ERA5	0.016	0.032	0.027	0.74	-	-	-	-
	GLDAS CLSM	-0.102	0.108	0.038	0.32	-	-	-	-



	GLDAS Noah	-0.122	0.127	0.037	0.49	-0.031	0.085	0.079	0.46
	GLDAS VIC	-0.013	0.049	0.047	0.39	-	-	-	-
	MERRA2	-0.113	0.118	0.034	0.50	-0.016	0.089	0.087	0.13
40cm	ERA5	0.108	0.111	0.025	0.69	-	-	-	-
	GLDAS CLSM	-0.018	0.028	0.022	0.44	-	-	-	-
	GLDAS Noah	-0.040	0.049	0.028	0.54	0.042	0.075	0.062	0.06
	GLDAS VIC	0.088	0.093	0.029	0.45	-	-	-	-
	MERRA2	-0.025	0.034	0.024	0.50	0.047	0.074	0.057	0.34
Soil temperature									
5cm	ERA5	-3.5	3.7	1.1	0.96	-2.4	3.0	1.8	0.84
	GLDAS CLSM	-3.1	3.4	1.3	0.94	-2.0	2.8	2.0	0.91
	GLDAS Noah	-3.5	3.9	1.8	0.89	-2.4	3.6	2.7	0.89
	GLDAS VIC	-4.3	4.4	1.2	0.95	-2.7	3.1	1.6	0.87
	MERRA2	-3.5	3.8	1.4	0.93	-2.6	3.3	2.0	0.91
20cm	ERA5	-5.0	5.0	0.7	0.98	-3.2	3.5	1.4	0.84
	GLDAS CLSM	-4.8	4.9	1.1	0.95	-3.0	3.4	1.7	0.87
	GLDAS Noah	-5.9	6.3	2.1	0.84	-2.9	3.3	1.6	0.88
	GLDAS VIC	-5.5	5.6	1.3	0.92	-3.8	4.1	1.5	0.85
	MERRA2	-5.1	5.2	1.0	0.95	-3.6	4.0	1.8	0.86
40cm	ERA5	-5.3	5.4	0.8	0.97	-2.8	3.0	1.2	0.79
	GLDAS CLSM	-5.1	5.2	0.8	0.97	-2.8	3.2	1.6	0.77
	GLDAS Noah	-6.2	6.5	1.9	0.85	-2.8	3.1	1.4	0.82
	GLDAS VIC	-5.7	5.8	1.1	0.93	-3.7	4.0	1.7	0.74
	MERRA2	-5.9	6.0	0.9	0.95	-3.3	3.8	1.8	0.70

711

712 **Table 5. Same as Table 4 but for the Shiquanhe network.**

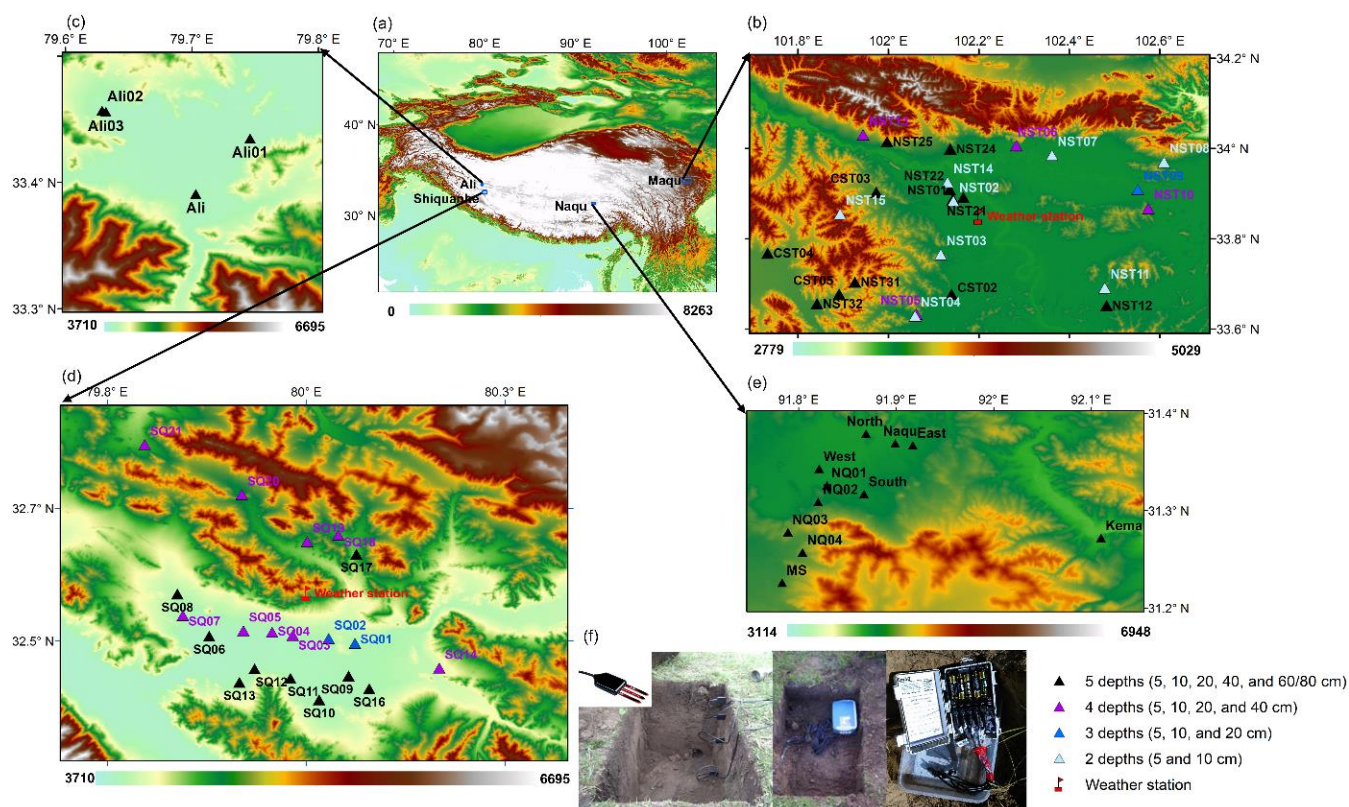
		Warm season				Cold season			
		Bias	RMSD	ubRMSD	R	Bias	RMSD	ubRMSD	R
Soil moisture									
5cm	ERA5	-0.001	0.060	0.060	0.80	-	-	-	-
	GLDAS CLSM	0.156	0.158	0.027	0.53	-	-	-	-
	GLDAS Noah	0.134	0.142	0.046	0.64	0.072	0.075	0.023	0.12
	GLDAS VIC	0.256	0.259	0.042	0.38	-	-	-	-
	MERRA2	0.070	0.082	0.042	0.73	0.060	0.065	0.024	0.13
20cm	ERA5	0.084	0.088	0.026	0.55	-	-	-	-
	GLDAS CLSM	0.152	0.153	0.021	0.56	-	-	-	-
	GLDAS Noah	0.159	0.161	0.025	0.66	0.145	0.146	0.008	0.28
	GLDAS VIC	0.256	0.259	0.042	0.31	-	-	-	-
	MERRA2	0.087	0.092	0.028	0.70	0.086	0.087	0.016	0.10
40cm	ERA5	0.107	0.110	0.021	0.30	-	-	-	-
	GLDAS CLSM	0.154	0.155	0.019	0.39	-	-	-	-
	GLDAS Noah	0.173	0.174	0.020	0.49	0.174	0.175	0.010	-0.19
	GLDAS VIC	0.272	0.274	0.032	0.29	-	-	-	-
	MERRA2	0.117	0.118	0.015	0.62	0.123	0.124	0.009	0.08
Soil temperature									
5cm	ERA5	-5.5	5.8	1.8	0.95	-6.2	7.0	3.3	0.83
	GLDAS CLSM	-5.9	6.2	1.6	0.96	-3.0	3.8	2.2	0.93
	GLDAS Noah	-4.7	5.0	1.6	0.96	-3.8	4.8	3.0	0.86
	GLDAS VIC	-11.8	12.2	3.1	0.84	-6.6	7.9	4.4	0.69
	MERRA2	-8.2	8.4	1.8	0.95	-5.5	5.8	1.9	0.95



20cm	ERA5	-6.6	6.8	1.7	0.94	-5.8	6.7	3.3	0.76
	GLDAS CLSM	-7.1	7.2	1.4	0.96	-3.2	3.8	2.1	0.92
	GLDAS Noah	-5.5	5.6	1.4	0.96	-2.9	4.1	2.9	0.83
	GLDAS VIC	-12.0	12.2	2.2	0.89	-7.2	8.1	3.7	0.71
	MERRA2	-9.2	9.4	1.6	0.95	-5.6	5.9	1.6	0.95
40cm	ERA5	-7.5	7.7	1.5	0.93	-6.1	6.8	2.9	0.75
	GLDAS CLSM	-8.9	9.0	1.3	0.96	-3.3	3.8	1.8	0.92
	GLDAS Noah	-6.6	6.7	1.4	0.95	-2.9	4.0	2.8	0.77
	GLDAS VIC	-12.8	12.9	1.7	0.92	-7.7	8.2	3.0	0.72
	MERRA2	-10.8	11.0	1.6	0.95	-5.9	6.0	1.4	0.95

713

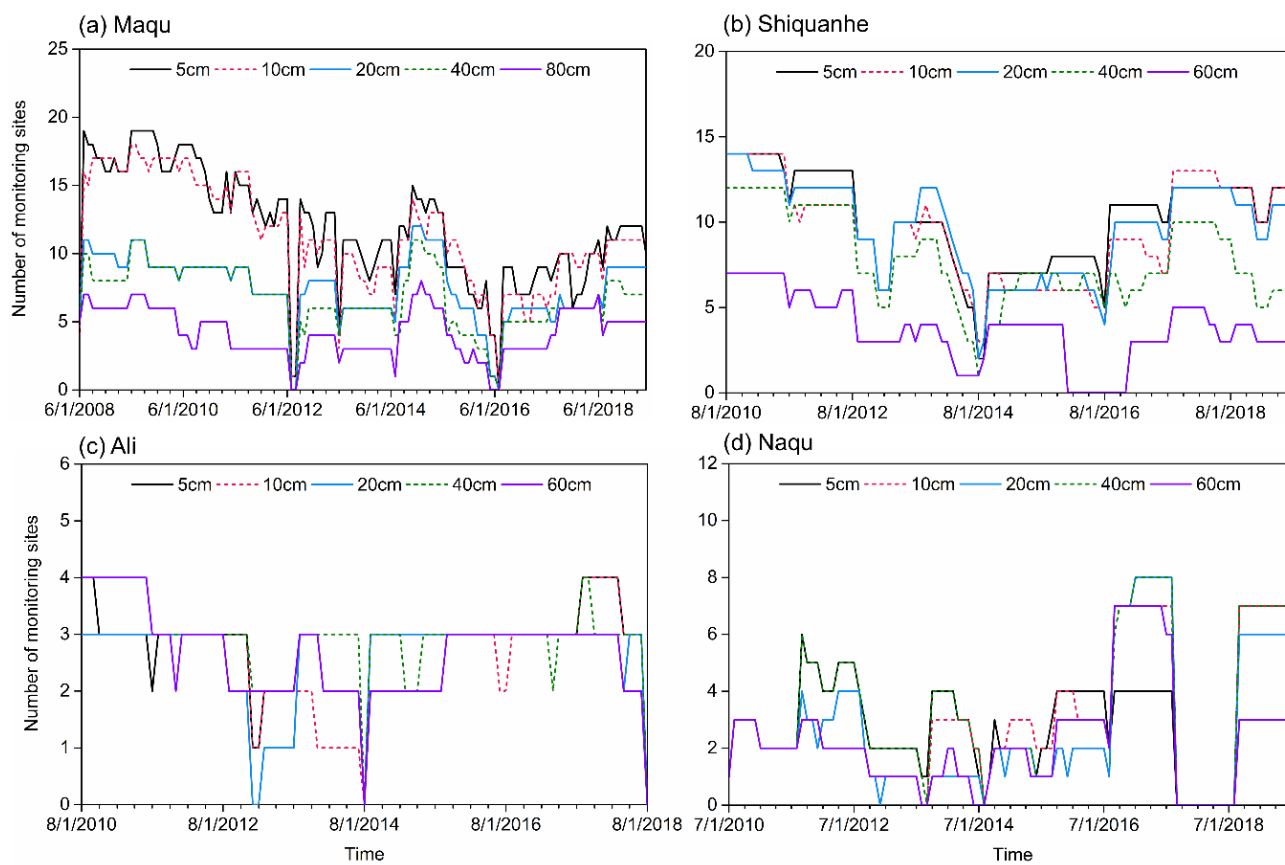
714



715

716 **Figure 1.** (a) Location of the Tibet-Obs network over the TP; Spatial distributions of SMST monitoring sites and weather station
 717 within the (b) Maqu, (c) Ali, (d) Shiquanhe, and (e) Naqu networks; and (f) an example of instruments configured for each SMST
 718 monitoring site. The triangles with different colours represent the SMST measured at different depths. (Base map is from EROS,
 719 Copyright: © EROS)

720

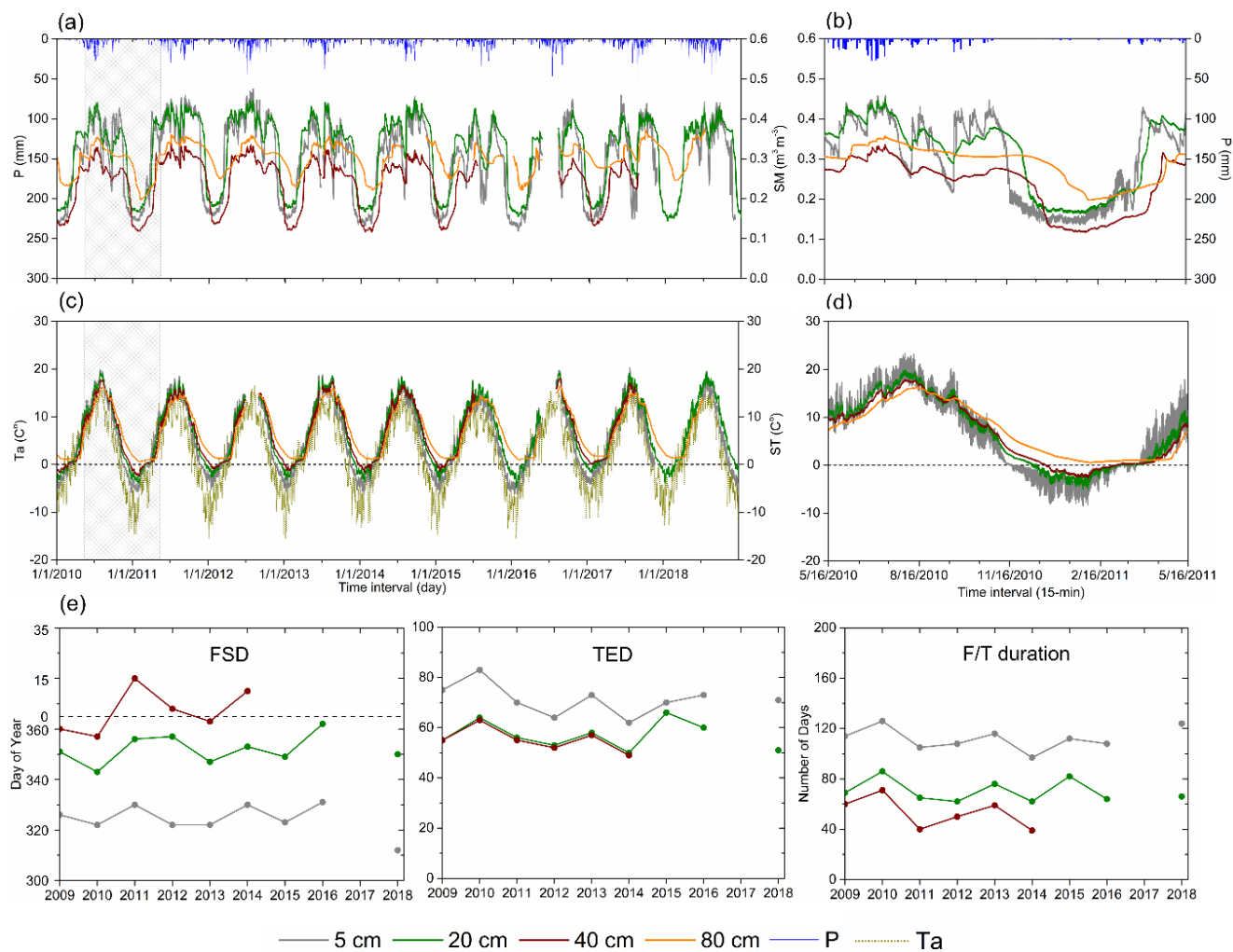


721

722 **Figure 2. Number of available SMST monitoring sites for different depths at each month for the (a) Maqu, (b) Shiquanhe, (c) Ali**
723 **and (d) Naqu networks.**

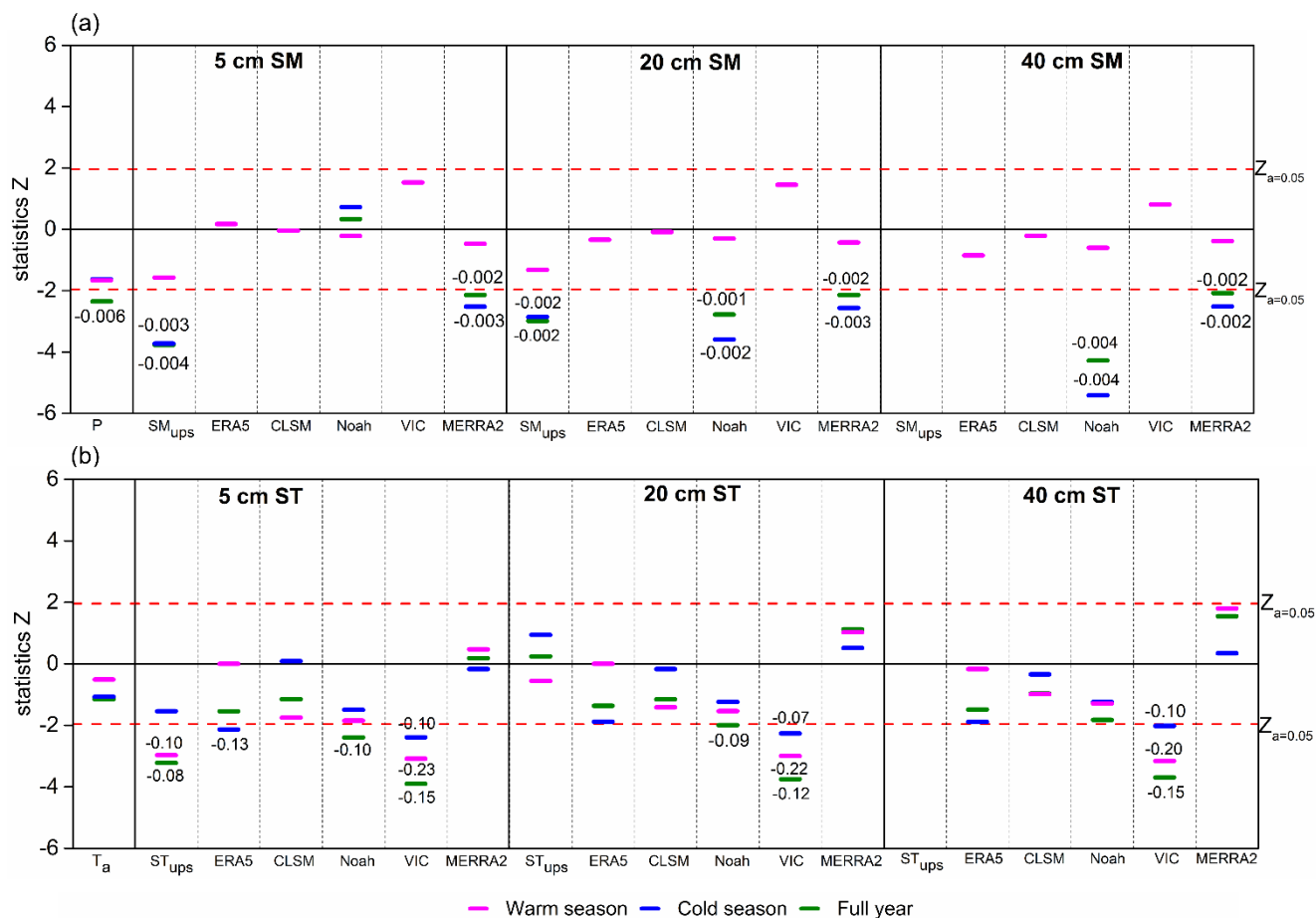
724

725



726

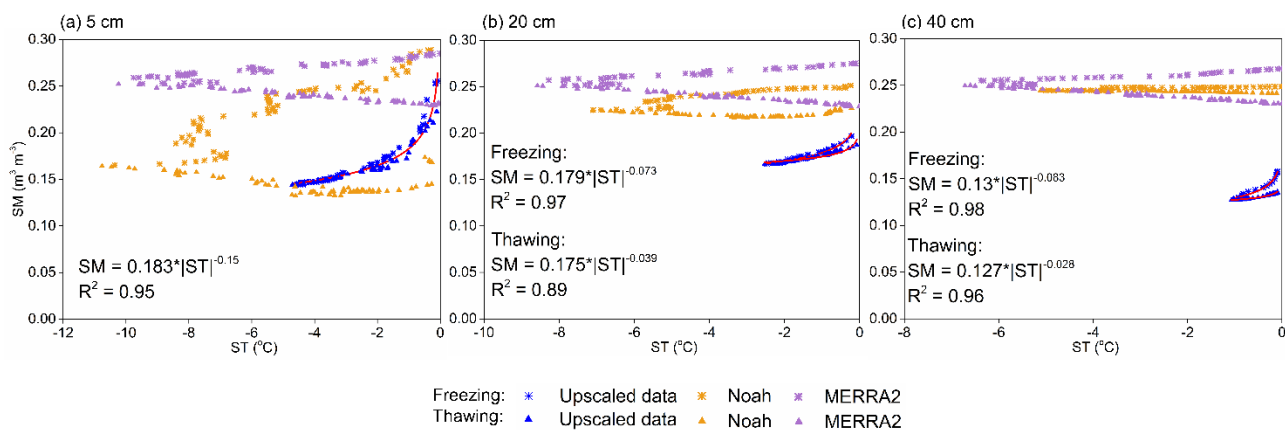
727 **Figure 3.** Time series of upscaled daily (a) SM_{ups} and (c) ST_{ups} at depths of 5, 20, 40, and 80 cm for the Maqu network between
 728 January 2010 and December 2018; the subplots highlight the time series of upscaled (b) SM_{ups} and (d) ST_{ups} with interval of 15-min
 729 between 16-5-2010 and 16-5-2011; and (e) annual variations of TSD, TED, and F/T duration at 5, 20, and 40 cm depths. The time
 730 series of daily precipitation and air temperature are shown in (a) and (c) as well.



731

732 **Figure 4. Mann Kendall trend test and Sen's slope estimate for the long-term (a) SM and (b) ST at depths of 5, 20 and 40 cm from**
 733 **2010 to 2018 obtained from the upscaled dataset and different model-based products for the Maqu network. The trend analysis**
 734 **results for the precipitation and air temperature are also shown in (a) and (b), respectively. The digits in the figure represent the**
 735 **values of Sen's slope estimate.**

736

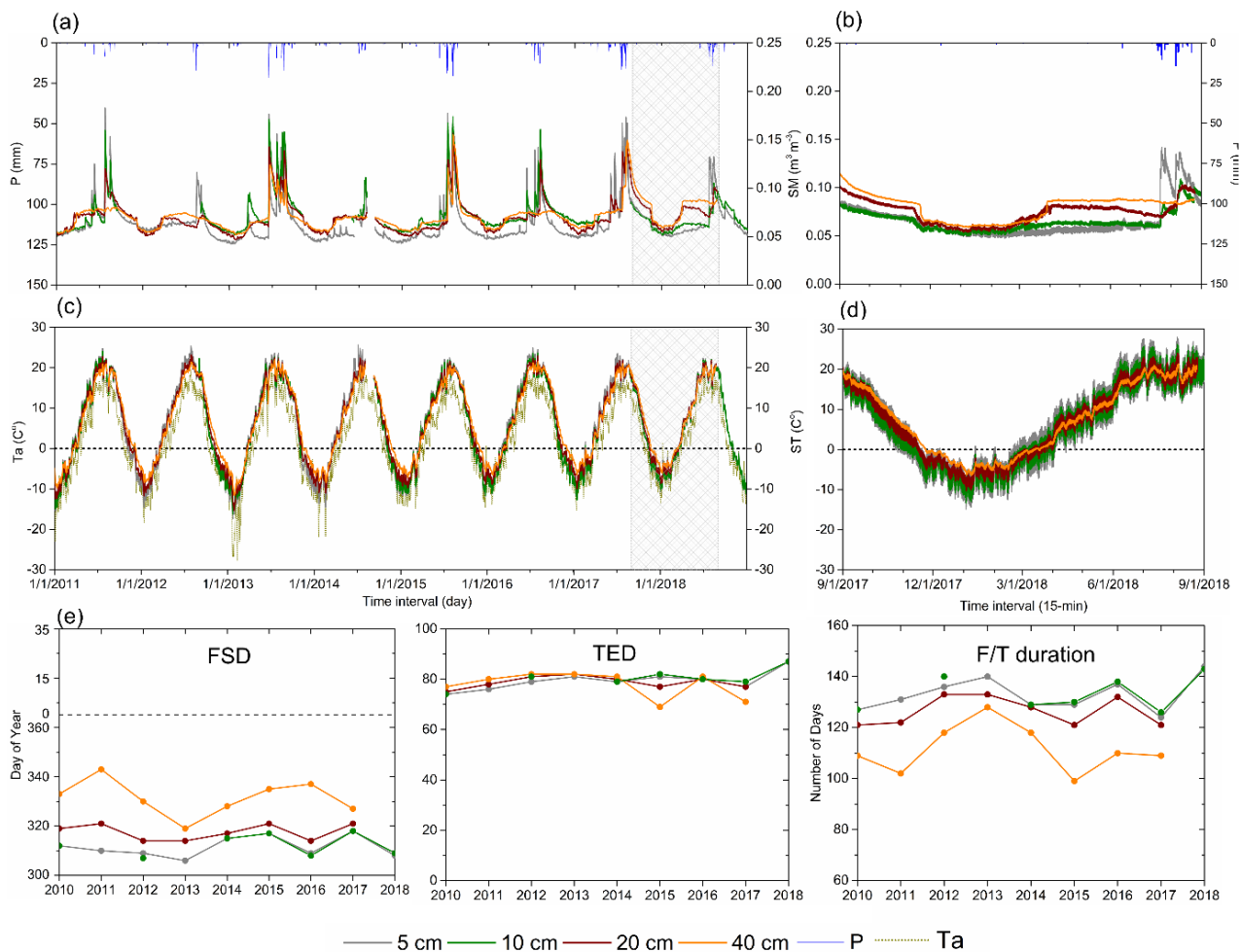


737

738 **Figure 5. Soil freezing characteristics for depths of (a) 5, (b) 20 and (c) 40 cm determined from the measured and simulated unfrozen**
739 **SM and subzero ST obtained from the upscaled dataset, GLDAS Noah and MERRA2 products for the Maqu network.**

740

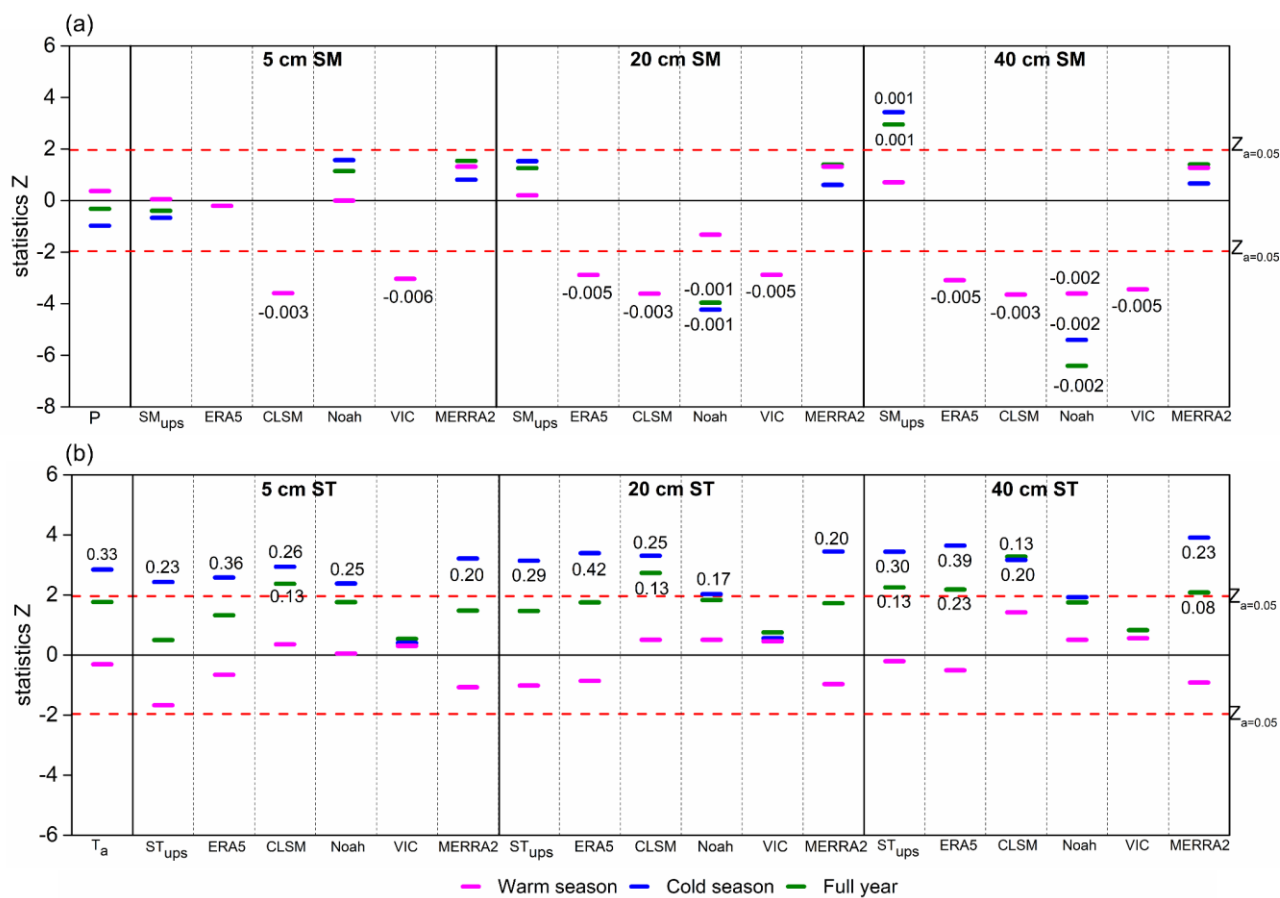
741



742

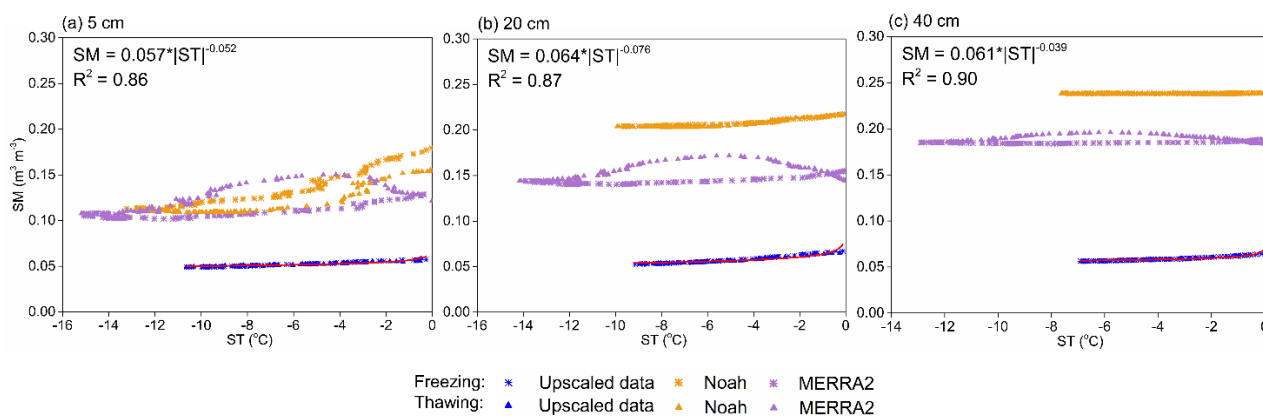
743 **Figure 6.** Time series of upscaled daily (a) SM_{ups} and (c) ST_{ups} at depths of 5, 10, 20, and 40 cm for the Shiquanhe network between
 744 January 2011 and December 2018; the subplots highlight the time series of upscaled (b) SM_{ups} and (d) ST_{ups} with interval of 15-min
 745 between 9-1-2017 and 8-31-2018; and (e) annual variations of TSD, TED, and F/T duration at 5, 10, 20, and 40 cm depths. The time
 746 series of daily precipitation and air temperature are shown in (a) and (c) as well.

747

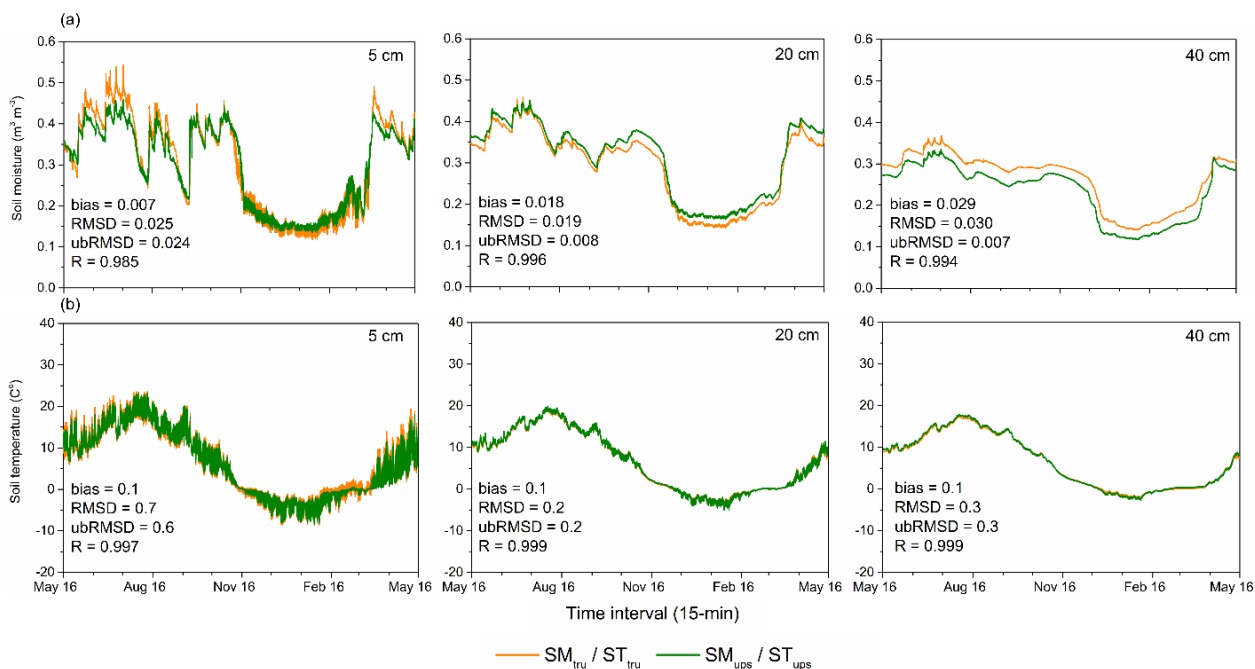


748
 749 **Figure 7.** Same as Figure 4 but for the Shiquanhe network from 2011 to 2018.

750



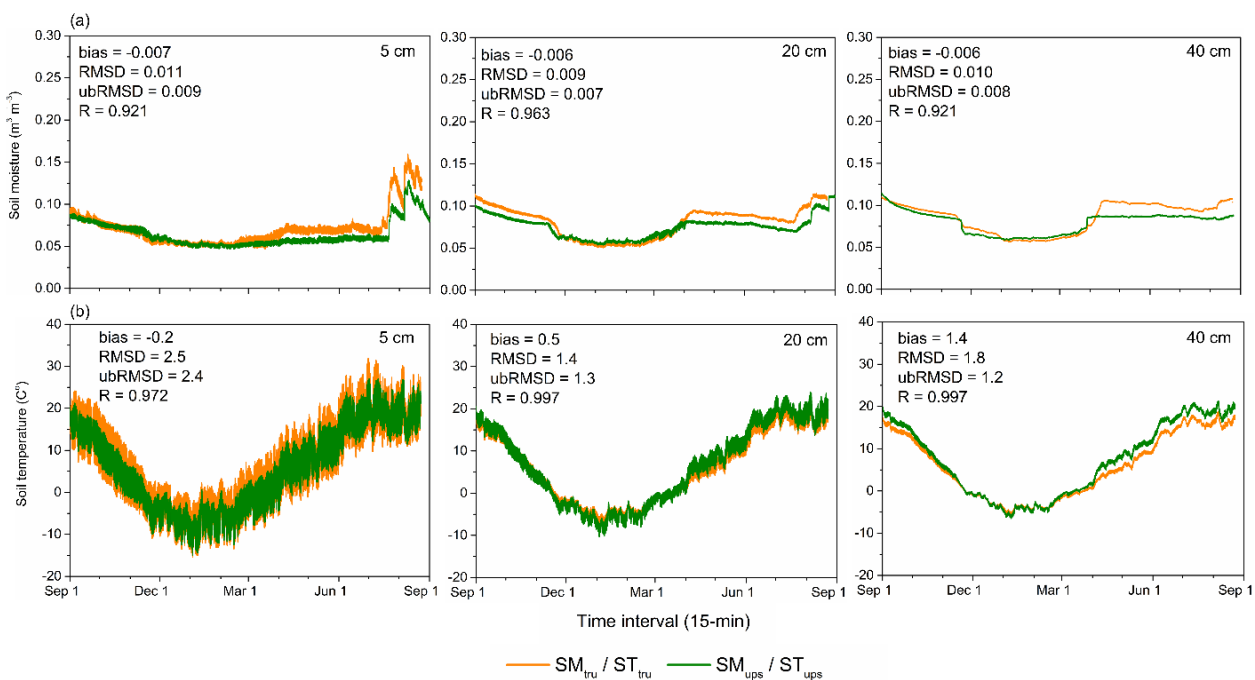
751
 752 **Figure 8.** Same as Figure 5 but for the Shiquanhe network.



753

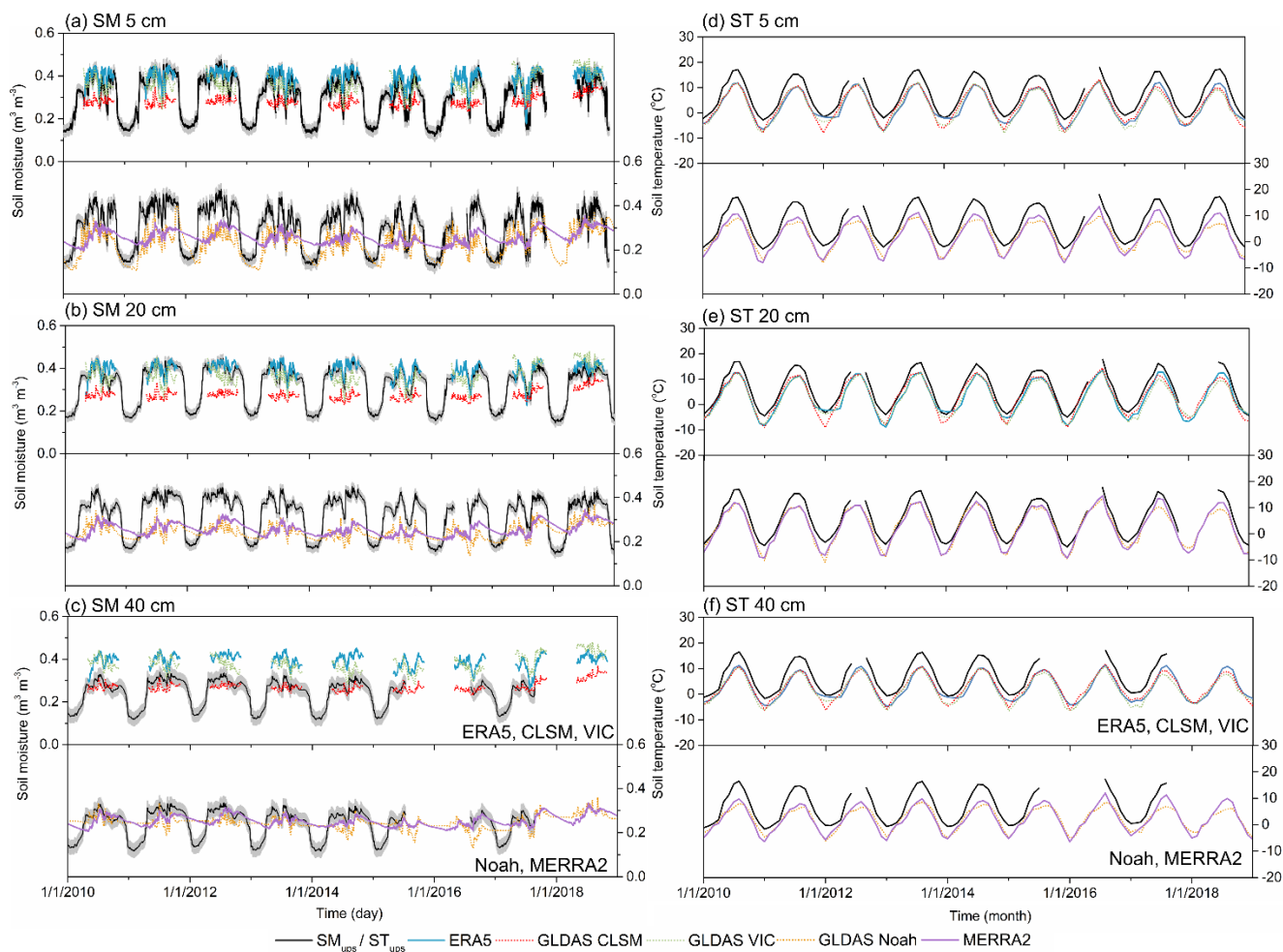
754 **Figure 9. Comparisons between the time series of (a) SM_{ups} and SM_{tru}, and (b) ST_{ups} and ST_{tru} at soil depths of 5, 20, and 40 cm with**
 755 **15-min interval from 16th May 2010 to 16th May 2011 for the Maqu network.**

756



757

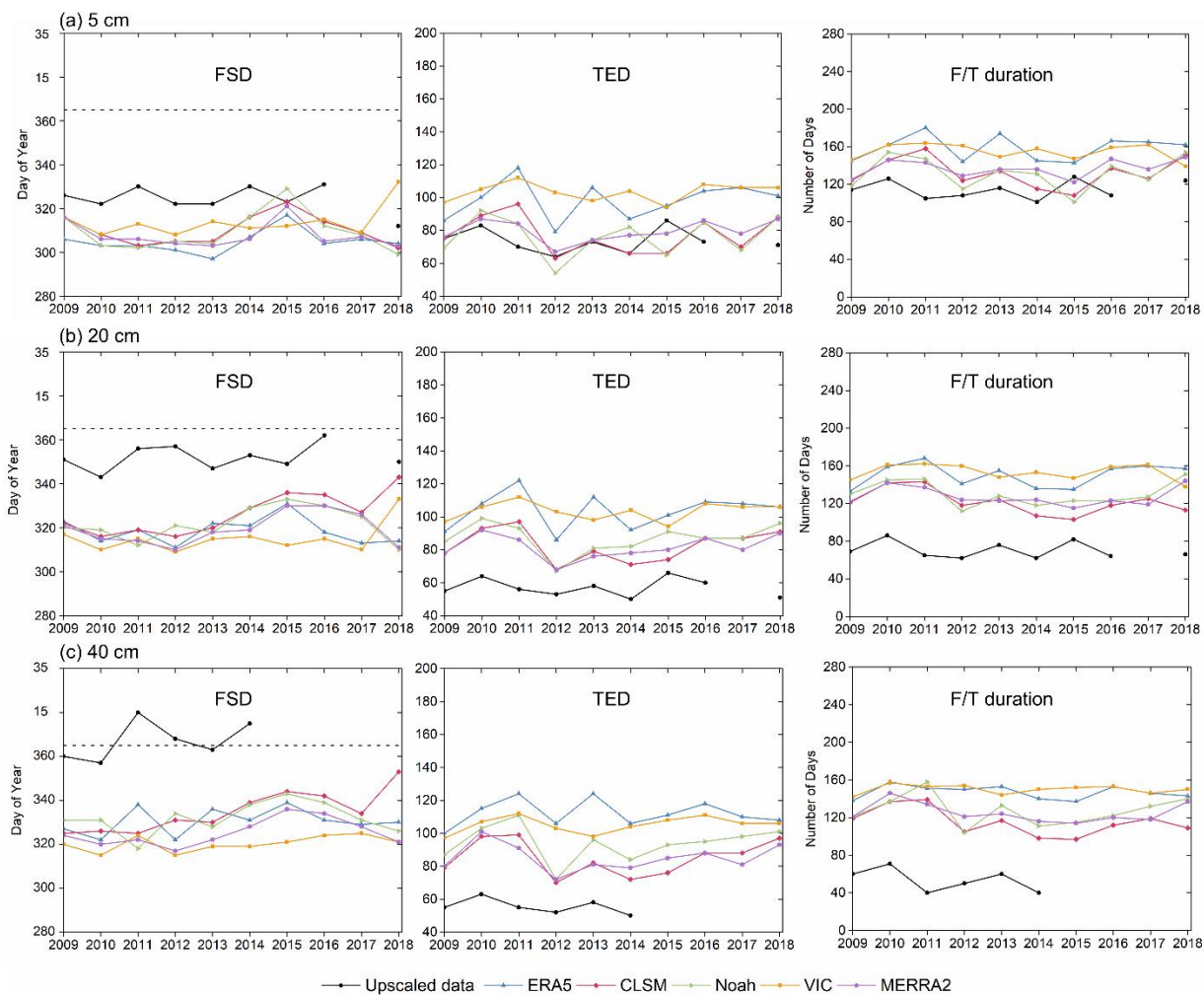
758 **Figure 10. Same as Figure 9 but for the Shiquanhe network from 1st Sep 2017 and 31st Aug 2018.**



759

760 **Figure 11.** Time series of daily average SM (a-c) and monthly mean ST (d-f) at soil depths of 5 (a, d), 20 (b, e), and 40 cm (c, f) derived
 761 from the upscaled SMST dataset and five model-based products from January 2010 to December 2018 for the Maqu network.

762

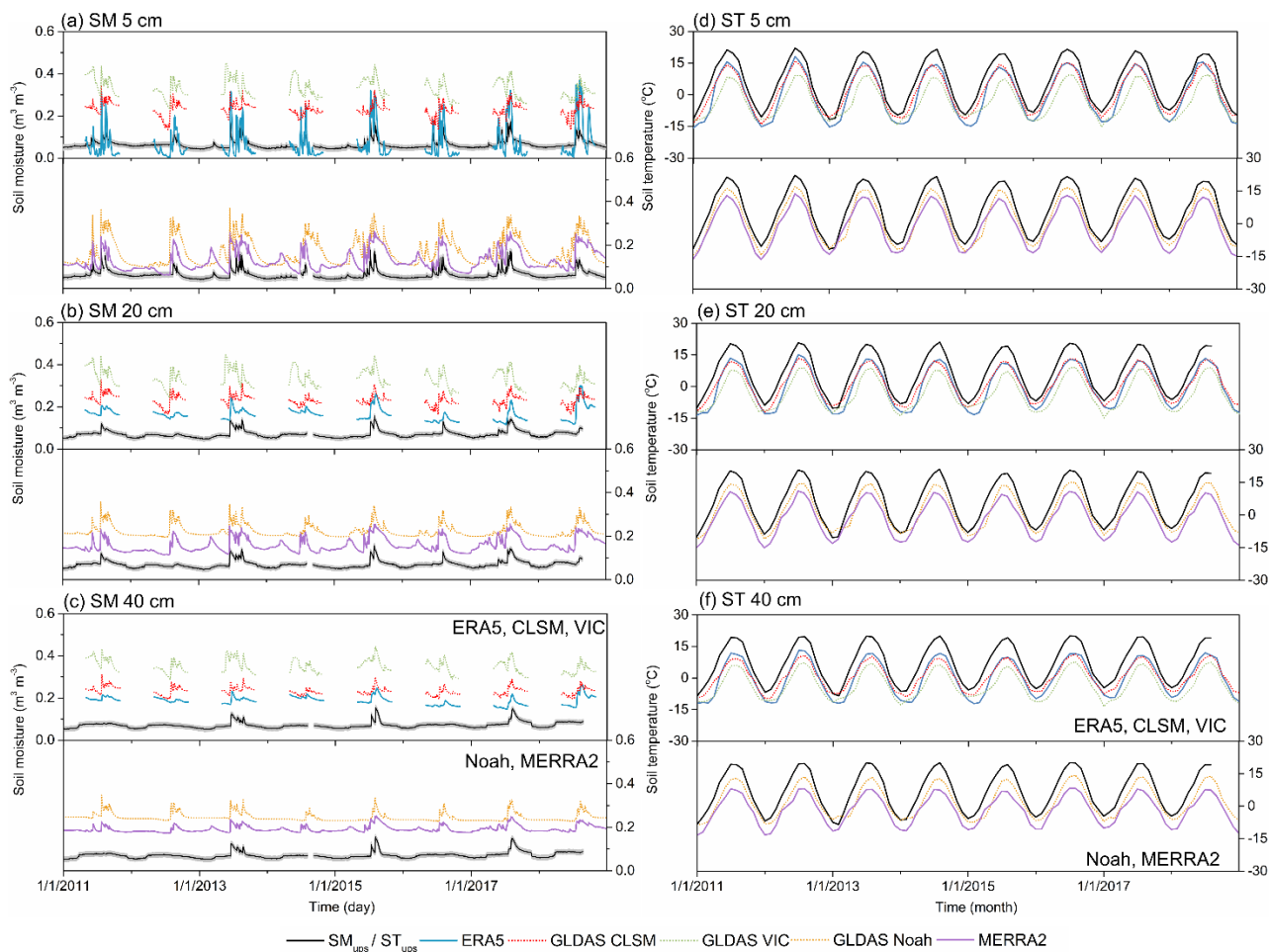


763

764 **Figure 12.** The annual variations of FSD, TED and F/T duration at the depth of (a) 5, (b) 20, and (c) 40 cm obtained from the
 765 upscaled dataset and five model-based products for the Maqu network.

766

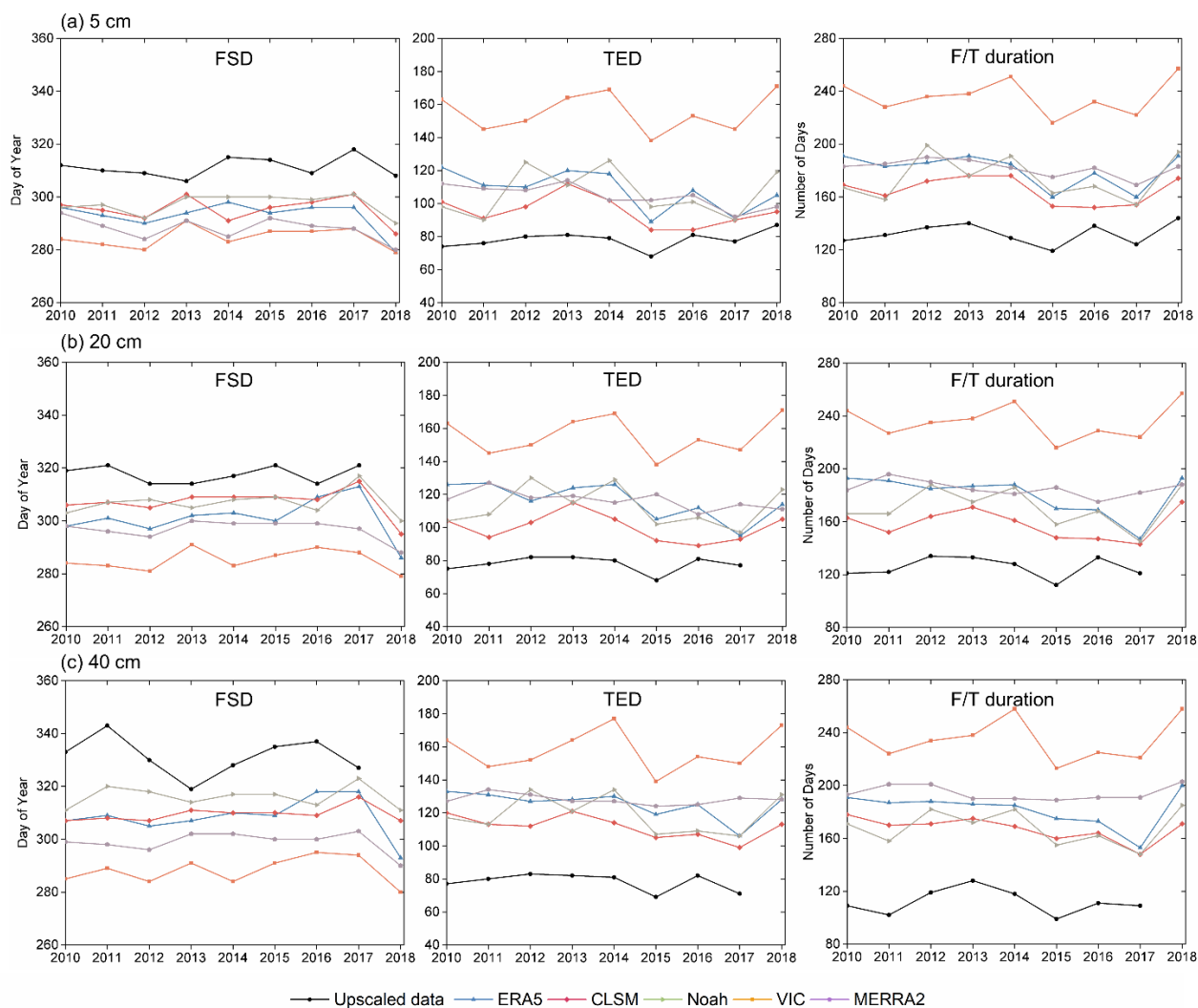
767



768

769 **Figure 13. Same as Figure 11 but for the Shiquanhe network from January 2011 to December 2018.**

770



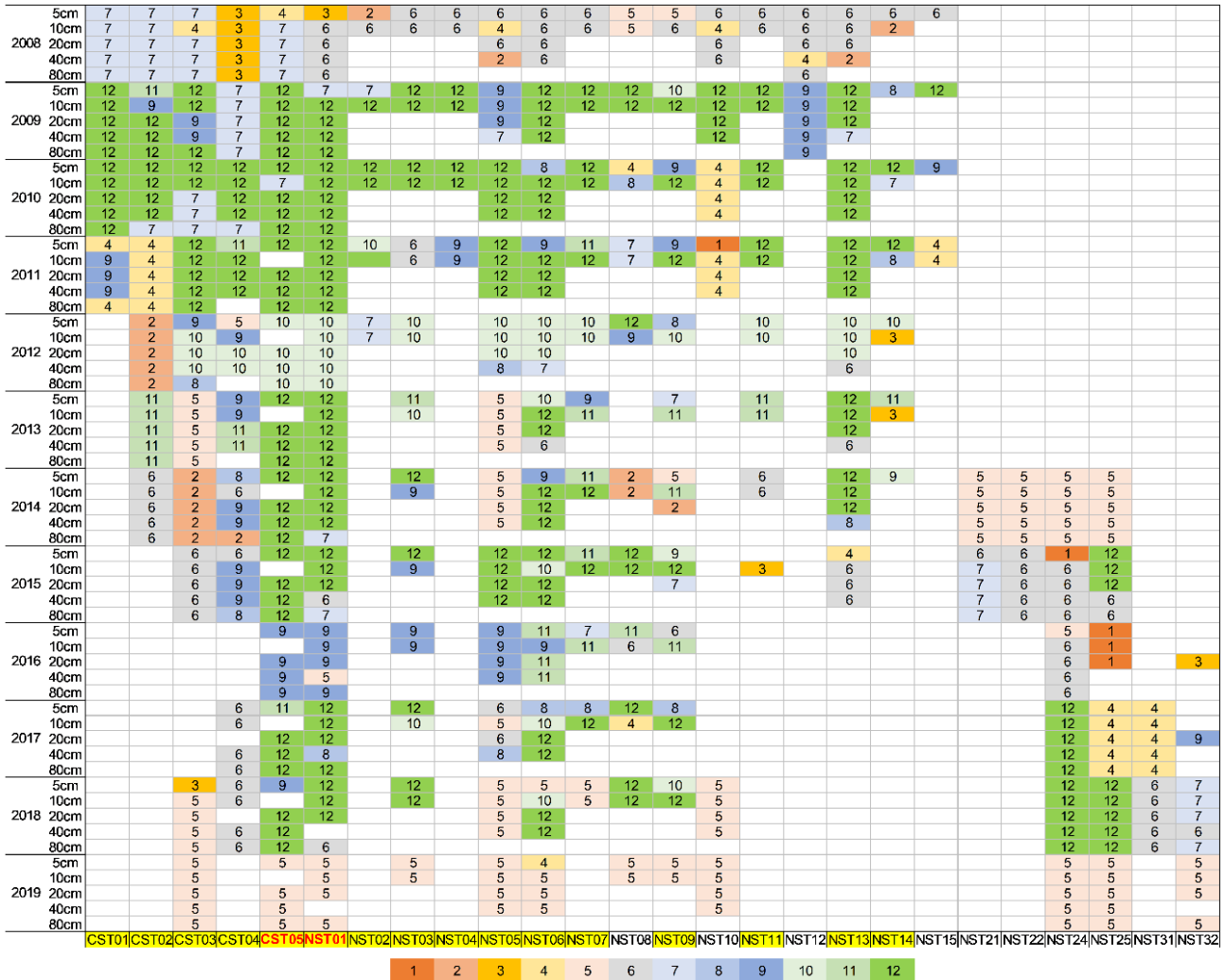
771

772 **Figure 14.** Same as Figure 8 but for the Shiquanhe network.

773

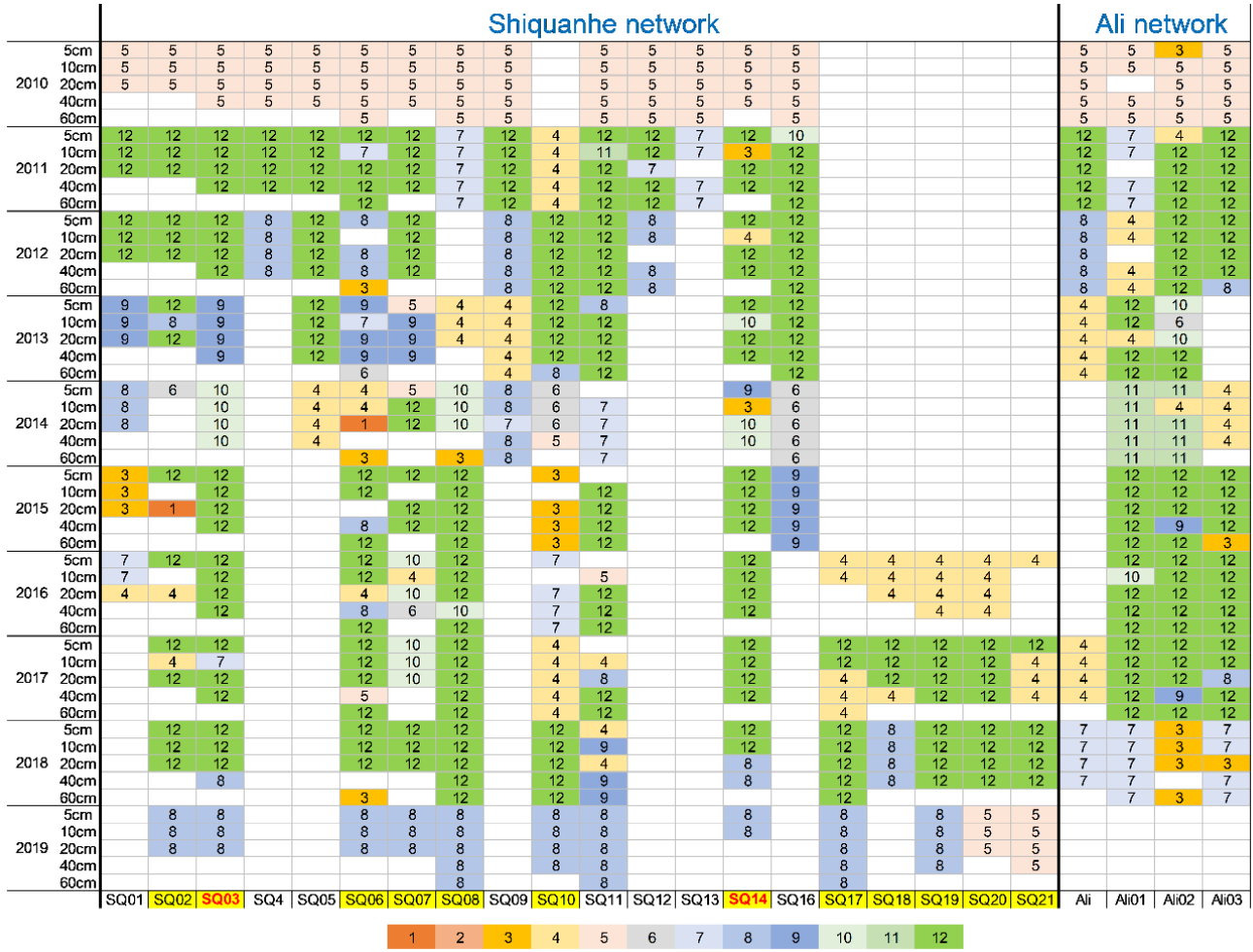


774 Appendix A: SMST data records of the Tibet-Obs



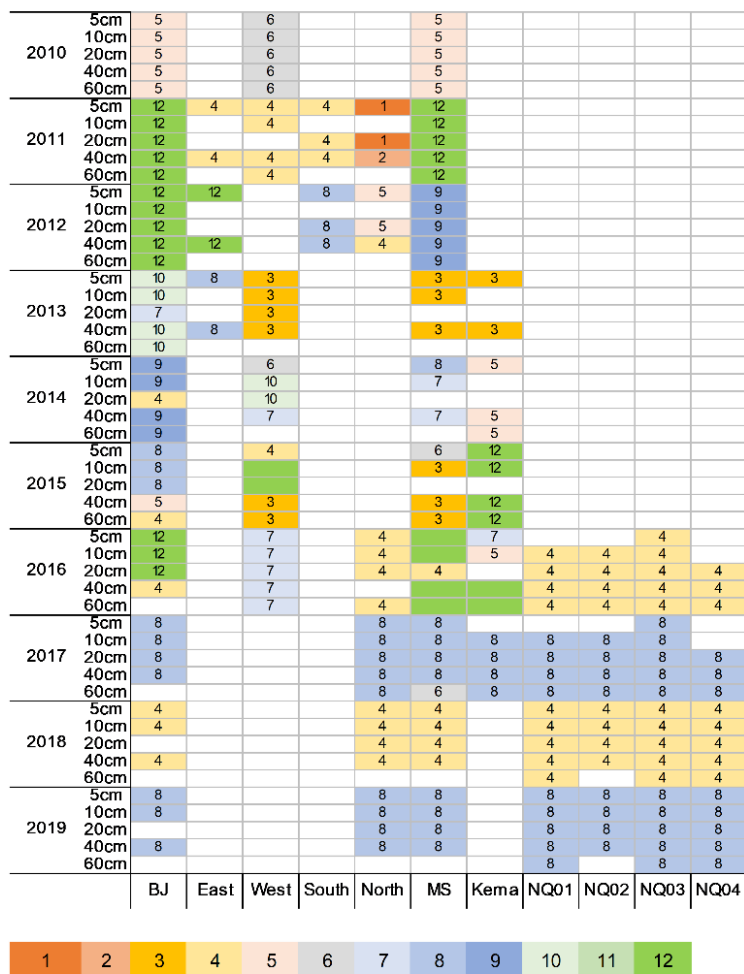
775 Figure A1. Data records of the SMST measured at different depths with temporal persistence from May 2008 to May 2019 (Y-axis)
 776 for all the monitoring sites in the Maqu network (X-axis). Cells with different colours and digits represent different number of
 777 months that contain valid SMST data in each year. Blank cells indicate that there are no measurements performed. Site names with
 778 highlight and red font represent the sites used for producing the long-term (May 2009 ~ May 2019) upscaled SMST dataset, and site
 779 names only with highlight represent the sites used for generating “ground truth” for a selected year (May 2010 ~ May 2011).

780



781
 782 **Figure A2.** Same as Table A1 but for the Ngari network with temporal persistence from August 2010 to August 2019. Site names
 783 **with highlight and red font** represent the sites used for producing the long-term (August 2010 ~ August 2019) upscaled SMST dataset,
 784 **and site names only with highlight** represent the sites used for generating “ground truth” for a selected year (August 2017 ~ August
 785 **2018)** in the Shiquanhe network.

786



787

788 **Figure A3.** Same as Table A1 but for the Naqu network with temporal persistence from June 2010 to August 2019.

789

790

791

792

793

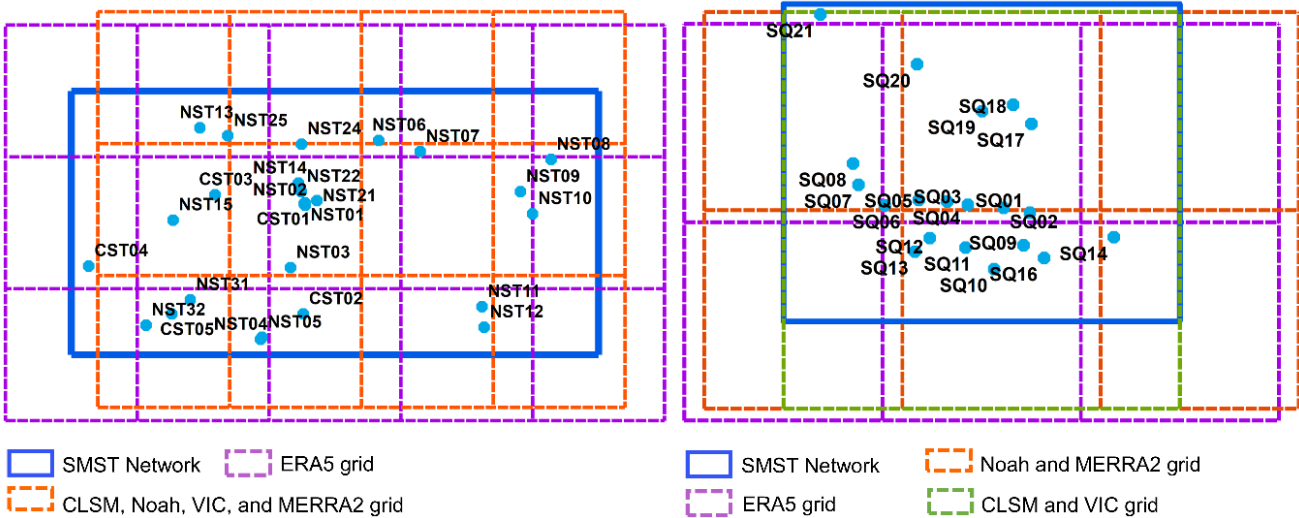
794



795 **Appendix B: Linear interpolation method for the model-based SMST data.**

(a) Maqu

(b) Shiquanhe



796

797 **Figure B1: Grids of the model-based products falling into the (a) Maqu and (b) Shiquanhe network areas (denoted by the colourful**
 798 **dashed rectangles).**

799 **B1 ERA5 SMST data**

800 The SMST derived from the ERA5 product for the depths of 5, 20, and 40 cm are calculated as:

801
$$X_{5,ERA5} \approx X_{0-7,ERA5}$$

802
$$X_{20,ERA5} \approx X_{7-28,ERA5} + (X_{28-100,ERA5} - X_{7-28,ERA5}) * (20 - 17.5)/(64 - 17.5)$$

803
$$X_{40,ERA5} \approx X_{7-28,ERA5} + (X_{28-100,ERA5} - X_{7-28,ERA5}) * (40 - 17.5)/(64 - 17.5)$$

804 where $X_{5,ERA5}$, $X_{20,ERA5}$, and $X_{40,ERA5}$ represent the interpolated SMST values at 5, 20, and 40 cm depths for the ERA5 product,
 805 and $X_{0-7,ERA5}$, $X_{7-28,ERA5}$, and $X_{28-100,ERA5}$ represent the SMST values for layers of 0-7, 7-28, 28-100 cm derived from the
 806 ERA5 product.

807

808 **B2 GLDAS-2.1 CLSM SMST data**

809 The SM derived from GLDAS-2.1 CLSM product for the depths of 5, 20, and 40 cm are calculated as:

810
$$X_{5,GLDAS\ CLSM} \approx X_{0-2,GLDAS\ CLSM}$$

811
$$X_{20,GLDAS\ CLSM} \approx X_{0-2,GLDAS\ CLSM} + (X_{0-100,GLDAS\ CLSM} - X_{0-2,GLDAS\ CLSM}) * (20 - 1)/(50 - 1)$$

812
$$X_{40,GLDAS\ CLSM} \approx X_{0-2,GLDAS\ CLSM} + (X_{0-100,GLDAS\ CLSM} - X_{0-2,GLDAS\ CLSM}) * (40 - 1)/(50 - 1)$$

813 The ST derived from GLDAS-2.1 CLSM product for the depths of 5, 20, and 40 cm are calculated as:

814
$$X_{5,GLDAS\ CLSM} \approx X_{0-10,GLDAS\ CLSM}$$



$$815 \quad X_{20,GLDAS\ CLSM} \approx X_{10-29,GLDAS\ CLSM} + (X_{29-68,GLDAS\ CLSM} - X_{10-29,GLDAS\ CLSM}) * (20 - 19.5)/(48.5 - 19.5)$$

$$816 \quad X_{40,GLDAS\ CLSM} \approx X_{10-29,GLDAS\ CLSM} + (X_{29-68,GLDAS\ CLSM} - X_{10-29,GLDAS\ CLSM}) * (40 - 19.5)/(48.5 - 19.5)$$

817

818 **B3 GLDAS-2.1 Noah SMST data**

819 The SMST derived from the GLDAS-2.1 Noah product for the depths of 5, 20, and 40 cm are calculated as:

$$820 \quad X_{5,GLDAS\ Noah} \approx X_{0-10,GLDAS\ Noah}$$

$$821 \quad X_{20,GLDAS\ Noah} \approx X_{0-10,GLDAS\ Noah} + (X_{10-40,GLDAS\ Noah} - X_{0-10,GLDAS\ Noah}) * (20 - 5)/(25 - 5)$$

$$822 \quad X_{40,GLDAS\ Noah} \approx X_{10-40,GLDAS\ Noah} + (X_{40-100,GLDAS\ Noah} - X_{10-40,GLDAS\ Noah}) * (40 - 25)/(70 - 25)$$

823

824 **B4 GLDAS-2.1 VIC SMST data**

825 The SMST derived from the GLDAS-2.1 VIC product for the depths of 5, 20, and 40 cm are calculated as:

$$826 \quad X_{5,GLDAS\ VIC} \approx X_{0-30,GLDAS\ VIC}$$

$$827 \quad X_{20,GLDAS\ VIC} \approx X_{0-30,GLDAS\ VIC} + (X_{30-130,GLDAS\ VIC} - X_{0-30,GLDAS\ VIC}) * (20 - 15)/(80 - 15)$$

$$828 \quad X_{40,GLDAS\ VIC} \approx X_{0-30,GLDAS\ VIC} + (X_{30-130,GLDAS\ VIC} - X_{0-30,GLDAS\ VIC}) * (40 - 15)/(80 - 15)$$

829

830 **B5 MERRA2 SMST data**

831 The SM derived from MERRA2 product for the depths of 5, 20, and 40 cm are calculated as:

$$832 \quad X_{5,MERRA2} \approx X_{0-5,MERRA2}$$

$$833 \quad X_{20,MERRA2} \approx X_{0-5,MERRA2} + (X_{0-100,MERRA2} - X_{0-5,MERRA2}) * (20 - 2.5)/(50 - 2.5)$$

$$834 \quad X_{40,MERRA2} \approx X_{0-5,MERRA2} + (X_{0-100,MERRA2} - X_{0-5,MERRA2}) * (40 - 2.5)/(50 - 2.5)$$

835 The ST derived from MERRA2 product for the depths of 5, 20, and 40 cm are calculated as:

$$836 \quad X_{5,MERRA2} \approx X_{0-10,MERRA2}$$

$$837 \quad X_{20,MERRA2} \approx X_{10-30,MERRA2}$$

$$838 \quad X_{40,MERRA2} \approx X_{10-30,MERRA2} + (X_{30-70,MERRA2} - X_{10-30,MERRA2}) * (40 - 20)/(50 - 20)$$

839

840 **Appendix C: Mann Kendall trend test and Sen's slope estimate**

841 Trend analysis for each time series is carried out as following steps:

842 1. Calculate month statistics (S_i)



843 For the i^{th} month (1~12), S_i is calculated as:

$$844 S_i = \sum_{K=1}^{Y-1} \sum_{L=K+1}^Y \text{sgn}(X_{i,L} - X_{i,K})$$

$$845 \text{sgn}(X_{i,L} - X_{i,K}) = \begin{cases} 1 & X_{i,L} > X_{i,K} \\ 0 & X_{i,L} = X_{i,K} \\ -1 & X_{i,L} < X_{i,K} \end{cases}$$

846 where $X_{i,L}$ and $X_{i,K}$ represent the monthly value of the data (e.g., SMST at different depths, precipitation, air temperature) for
 847 the K^{th} and L^{th} year (satisfied $1 \leq K \leq Y-1$, $K \leq L \leq Y$), Y represents the total number of years (e.g., 9 for the Maqu network
 848 and 8 for the Shiquanhe network).

849 2. Calculate the variance of S_i ($VAR(S_i)$)

850 For the i^{th} month (1~12), $VAR(S_i)$ is calculated as:

$$851 VAR(S_i) = \frac{1}{18} [Y(Y-1)(2Y+5) - \sum_{p=1}^{g_i} t_{i,p}(t_{i,p}-1)(2t_{i,p}+5)]$$

852 where g_i is the total number of equal-value data point group, and $t_{i,p}$ is the number of equal-value data point in the p^{th} group.

853 3. Calculate the seasons statistic and its variance (S and $VAR(S)$)

854 For the fully year, cold seasons, and warm seasons, S and $VAR(S)$ are calculated as:

$$855 S = \sum S_i$$

$$856 VAR(S) = \sum VAR(S_i)$$

857 where i denotes 1~12 for the full year, 5~10 for the warm season, and 1~4, 11, and 12 for the cold seasons.

858 4. Calculate the final statistic (Z)

859 The final statistics Z for the full year, cold seasons, and warm seasons is calculated as:

$$860 Z = \begin{cases} \frac{S-1}{\sqrt{VAR(S)}} & \text{if } S > 0 \\ 0 & \text{if } S = 0 \\ \frac{S+1}{\sqrt{VAR(S)}} & \text{if } S < 0 \end{cases}$$

861 If the final statistics Z is positive (negative) and its absolute value is greater than $Z_{1-\alpha/2}$ (here $\alpha = 0.05$, $Z_{1-\alpha/2} = 1.96$), the
 862 time series showed uptrend (downtrend) at the significance level of α . Otherwise, there is no significant trend existed.

863 5. Sen's slope estimate

864 If there is a trend existed, we will further estimate the trend slope using Sen's method. For the i^{th} month, individual slope Q_i is
 865 calculated as:

$$866 Q_i = \frac{X_{i,L} - X_{i,K}}{L - K}$$

867 where i denotes 1~12 for the full year, 5~10 for the warm season, and 1~4, 11, and 12 for the cold seasons. The median value
 868 of the Q_i is considered as the Sen's trend slope.

869